Unified modelling of near-cathode plasma layers in high-pressure arc discharges

IOP PUBLISHING JOURNAL OF PHYSICS D: APPLIED PHYSICS

J. Phys. D: Appl. Phys. **41** (2008) 245201 (26pp) doi:10.1088/0022-3727/41/24/245201

Unified modelling of near-cathode plasma layers in high-pressure arc discharges

N A Almeida[1], M S Benilov[1] and G V Naidis[2]

[1] Departamento de Física, Universidade da Madeira, 9000 Funchal, Portugal
[2] Institute for High Temperatures of the Russian Academy of Sciences, Moscow 125412, Russia

Received 28 May 2008, in final form 14 August 2008
Published 25 November 2008
Online at stacks.iop.org/JPhysD/41/245201

Abstract

A model of a near-cathode region in high-pressure arc discharges is developed in the framework of the hydrodynamic (diffusion) approximation. Governing equations are solved numerically in 1D without any further simplifications, in particular, without explicitly dividing the near-cathode region into a space-charge sheath and a quasi-neutral plasma. Results of numerical simulation are reported for a very high-pressure mercury arc and an atmospheric-pressure argon arc. Physical mechanisms dominating different sections of the near-cathode region are identified. It is shown that the near-cathode space-charge sheath is of primary importance under conditions of practical interest. Physical bases of simplified models of the near-cathode region in high-pressure arc discharges are analysed. A comparison of results given by the present model with those given by a simplified model has revealed qualitative agreement; the agreement is not only qualitative but also quantitative in the case of an atmospheric-pressure argon plasma at moderate values of the near-cathode voltage drop. The modelling data are compared with results of spectroscopic measurements of the electron temperature and density in the near-cathode region.

(Some figures in this article are in colour only in the electronic version)

1. Introduction

It has long been realized that an adequate description of the near-cathode plasma layer is the key element of the theory of plasma–cathode interaction in high-pressure arc discharges. There are many works treating near-cathode plasma layers (see, e.g., [1–15]; a review and further references can be found in [16]). However, there is still no universally accepted understanding of the physics involved. Neither are there universally employed simulation models. In part, the unsatisfactory state of the theory is due to diversity of the physical mechanisms involved and complexity of the overall physical picture. On the other hand, near-cathode layers of high-pressure arc discharges represent an extremely difficult object for experimental investigation due to their very small dimensions and extreme conditions typical of arc discharges. Therefore, the experiment cannot provide much guidance for the theory.

Published papers deal with different aspects of near-cathode plasma layers and employ different approaches; however, all of them have one point in common: the near-cathode plasma layer is *a priori* divided into a number of sub-layers with different properties (such as a layer of thermal non-equilibrium, an ionization layer, a near-cathode space-charge sheath, etc), each sub-layer is described by its own set of equations and solutions in adjacent sub-layers are matched in some way or other at a boundary between the sub-layers. The division of the near-cathode plasma layer into sub-layers with different properties reflects the fact that different physical mechanisms in many cases, although not always, come into play on different length scales. However, the usage of this division as a basis for a calculation model inevitably involves quite a bit of intuitive consideration and therefore is not a proper way to develop commonly accepted physical understanding and/or simulation models. In fact, there is no universally accepted point of view even on such a basic question as to what sub-layers are the most important and must be necessarily included in a model: while most of the workers believe that a near-cathode space-charge sheath is of primary importance, there are models, also recent ones, in which a space-charge sheath is discarded; see [16] and references therein.

An alternative to the above-described approach relying on an *a priori* introduction of different sub-layers is to model

the whole of a near-cathode region in the framework of a single set of equations without simplifying assumptions such as thermal equilibrium, ionization (Saha) equilibrium and quasi-neutrality. After such modelling has been completed, one will be able to identify physical mechanisms dominating different regions and thus pin down appropriate sub-layers. (In other words, the introduction of sub-layers, while being hardly justifiable as a basis of a numerical model, is natural and legitimate as a tool of analysis of results of calculations in which the near-cathode plasma layer is treated in a unified way.) In spite of being highly desirable, unified numerical modelling of near-cathode plasma layers in high-pressure arc discharges still has not been reported, the likely reason being the considerable computational complexity of the problem. Note that a two-dimensional modelling of high-pressure arc plasmas without assumptions of thermal or ionization equilibrium has been performed in [17, 18]; however, the assumption of quasi-neutrality is more difficult to relax since this amounts to solving the Poisson equation in the whole near-cathode region, including its outer part where the density of the charged particles is quite high and so is the degree of quasi-neutrality. On the other hand, in [19] boundary layers of a high-pressure combustion plasma with an alkali seed were modelled in the framework of a one-dimensional (1D) approach without assumptions of thermal or ionization equilibrium or quasi-neutrality, however only for conditions of low current densities and, consequently, low ionization degree.

In this work, a unified 1D modelling of near-cathode plasma layers is performed in the range of (high) current densities from 10^6 to 10^8 A m^{-2}, which are typical for cathodes of high-pressure arc discharges. Detailed calculation results are given for an argon arc at atmospheric pressure, which is a kind of a standard high-pressure arc, and a mercury arc at the pressure of 100 bar, which is typical for high-intensity discharge lamps. Dominating physical mechanisms are elucidated and the validity of assumptions is analysed on which available simplified models are based.

Distribution functions of the ions and the electrons in the bulk of a near-cathode region of a high-pressure arc discharge are close to the Maxwellian ones due to frequent ion–ion, ion–neutral atom and electron–electron collisions. Therefore, the bulk of the near-cathode region of a high-pressure arc discharge can be adequately described by conventional hydrodynamic (diffusion) equations. The situation is different in a very thin section of a near-cathode region immediately adjacent to the cathode surface, where deviations from the Maxwell distribution can occur. Hence, equations more complex than conventional hydrodynamic equations may be needed in a general case in order to uniformly describe the whole of a near-cathode region. For example, one may need to supplement a conventional hydrodynamic transport equation for the ions, which takes into account diffusion and drift of the ions and momentum exchange between the ion and atom species in elastic collisions, with terms accounting for ion inertia and momentum exchange between the ion and atom species due to ionization and recombination as was done in [2, 5, 10, 13, 15], or to supplement a set of governing equations with a kinetic equation for the isotropic part of the electron distribution function involving both a derivative in the energy space and a spatial derivative, as it was done in [20] in simulations of a near-cathode region in a high-pressure combustion plasma with an alkali seed. However, such complications are hardly advisable at the very first step. In this work, a unified modelling of near-cathode plasma layers in arc discharges is performed on the basis of conventional hydrodynamic equations. This approach is well justified for arcs in high-intensity discharge lamps and should also give acceptable accuracy for atmospheric-pressure argon arcs provided that the near-cathode voltage drop is not too high.

The outline of the paper is as follows. In section 2 governing equations of the model are given, together with corresponding boundary conditions. Results of calculation are given and discussed in section 3. A comparison with the experiment is discussed in section 4 and conclusions are summarized in section 5. The paper contains two appendices, describing evaluation of transport, kinetic and radiation coefficients and the method of numerical solution.

2. The model

2.1. The system of equations

Let us consider a near-cathode region of an arc discharge in an atomic gas under high pressure, of the order of atmospheric or higher. Convective effects in the near-cathode region are neglected. The plasma comprises neutral atoms, ions and electrons; the presence of multiply charged ions is neglected as justified in [6]. The atoms and ions have the same temperature T_h which is in a general case different from the electron temperature T_e.

The system of equations governing spatial distributions of plasma parameters in the near-cathode region is as follows. Equations of conservation of species read

$$\nabla \cdot \boldsymbol{J}_\alpha = \omega_\alpha, \qquad \alpha = \mathrm{i, e, a}, \tag{1}$$

Here $\boldsymbol{J}_\alpha$ is the number density of transport flux of the species α ($\boldsymbol{J}_\alpha = n_\alpha \boldsymbol{v}_\alpha$, where n_α and $\boldsymbol{v}_\alpha$ are the number density and mean velocity of particles of the species α), ω_α is the net rate of production of particles of the species α in volume reactions and indices i, e, a refer to ions, electrons and atoms, respectively. The dominating ionization mechanism in atomic plasmas is ionization in collisions with electrons and the dominating recombination mechanism is recombination with an electron acting as a third body, then

$$\omega_\mathrm{i} = \omega_\mathrm{e} = -\omega_\mathrm{a} = k_\mathrm{i} n_\mathrm{a} n_\mathrm{e} - k_r n_\mathrm{i} n_\mathrm{e}^2, \tag{2}$$

where k_i and k_r are the ionization and recombination rate constants. Evaluation of these constants and all the other transport, kinetic and radiation coefficients is described in appendix A.

Adding equations (1) for the ions and the atoms, one arrives at the equation of conservation of nuclei

$$\nabla \cdot (\boldsymbol{J}_\mathrm{i} + \boldsymbol{J}_\mathrm{a}) = 0. \tag{3}$$

Subtraction of equation (1) for the electrons from that for the ions gives

$$\nabla \cdot (\boldsymbol{J}_\mathrm{i} - \boldsymbol{J}_\mathrm{e}) = 0. \tag{4}$$

Since $\boldsymbol{J}_\mathrm{i} - \boldsymbol{J}_\mathrm{e} = \boldsymbol{j}/e$, where $\boldsymbol{j}$ is the density of electric current, equation (4) has the meaning of equation of continuity of electric current. In the following, equations (3) and (4) will be used instead of equation (1) for the ions and the atoms.

If the ionization degree of a plasma is low enough, transport of plasma species may be described by means of Fick's law written for the ions and the electrons, the so-called drift–diffusion approximation (e.g. [21]). Since plasmas in arc discharges are frequently strongly or even fully ionized, the use of Fick's law in this work would be inappropriate and transport equations taking the multicomponent diffusion into account must be used instead. Such equations are derived in the kinetic theory of gases, e.g. [22–26]. When resolved with respect to diffusion forces, they are called Stefan–Maxwell equations and may be written as [25]

$$-\nabla p_\alpha + n_\alpha e Z_\alpha \boldsymbol{E} + \frac{\rho_\alpha}{\rho}[\nabla p - e(n_\mathrm{i} - n_\mathrm{e})\boldsymbol{E}] - \sum_\beta \frac{n_\alpha n_\beta k T_{\alpha\beta} C_{\alpha\beta}}{n D_{\alpha\beta}}(\boldsymbol{v}_\alpha - \boldsymbol{v}_\beta) - \boldsymbol{R}_\alpha^\mathrm{T} = 0, \tag{5}$$

where

$$m_{\alpha\beta} = \frac{m_\alpha m_\beta}{m_\alpha + m_\beta}, \qquad T_{\alpha\beta} = \frac{m_\alpha T_\beta + m_\beta T_\alpha}{m_\alpha + m_\beta}. \tag{6}$$

Here $\alpha, \beta = \mathrm{i}, \mathrm{e}, \mathrm{a}$; m_α, T_α, $\rho_\alpha = n_\alpha m_\alpha$ and $p_\alpha = n_\alpha k T_\alpha$ are the particle mass, temperature, mass density and partial pressure of the species α (we recall that $T_\mathrm{i} = T_\mathrm{a} = T_\mathrm{h} \neq T_\mathrm{e}$); $n = \sum_\beta n_\beta$, $\rho = \sum_\beta \rho_\beta$ and $p = \sum_\beta p_\beta$ are the total number and mass densities and pressure of the plasma; $D_{\alpha\beta}$ are binary diffusion coefficients evaluated in the first approximation in expansion in the Sonine polynomials in the method of Chapman–Enskog and $C_{\alpha\beta}$ are coefficients of the order unity introducing corrections arising in higher approximations (note that $D_{\beta\alpha} = D_{\alpha\beta}$, $C_{\beta\alpha} = C_{\alpha\beta}$); $m_{\alpha\beta}$ and $T_{\alpha\beta}$ are the reduced mass and temperature; terms $\boldsymbol{R}_\alpha^\mathrm{T}$ account for thermal diffusion; $\boldsymbol{E}$ is the electric field. Note that equations (5) may be viewed in a simplified way as equations of conservation of momentum of species written under the assumption that the inertia forces are negligible, with the first, second and fourth terms on the left-hand side of equations (5) having the meaning of, respectively, the pressure gradient of the species α, the force exerted over this species by the electric field and the resultant force of friction between this species and the other ones.

The thermal diffusion forces $\boldsymbol{R}_\alpha^\mathrm{T}$ are given by formulae

$$\boldsymbol{R}_\alpha^\mathrm{T} = C_\alpha^{(\mathrm{h})} n_\alpha k \nabla T_\mathrm{h} + C_\alpha^{(\mathrm{e})} n_\alpha k \nabla T_\mathrm{e}, \qquad \boldsymbol{R}_\mathrm{e}^\mathrm{T} = C_\mathrm{e}^{(\mathrm{e})} n_\mathrm{e} k \nabla T_\mathrm{e} \tag{7}$$

for heavy-particle species ($\alpha = \mathrm{i}, \mathrm{a}$) and for electrons, respectively. (Note that the transport equation for electrons does not contain a term with ∇T_h since the corresponding force is negligibly small due to the smallness of the electron-to-ion mass ratio [25].) The thermal diffusion coefficients $C_\alpha^{(\mathrm{h})}$ and $C_\alpha^{(\mathrm{e})}$ satisfy equalities

$$n_\mathrm{a} C_\mathrm{a}^{(\mathrm{h})} + n_\mathrm{i} C_\mathrm{i}^{(\mathrm{h})} = 0, \qquad \sum_\alpha n_\alpha C_\alpha^{(\mathrm{e})} = 0. \tag{8}$$

Equations (5) are interdependent (summation of these equations over α gives a trivial result); therefore any one of them may be dropped. We will drop the equation for atoms.

The assumption of negligible convection requires that the force exerted by the electric field over the plasma be compensated by the plasma pressure gradient:

$$-\nabla p + e(n_\mathrm{i} - n_\mathrm{e})\boldsymbol{E} = 0. \tag{9}$$

It follows, in particular, that the third term on the left-hand side of equations (5) vanishes.

The electron and heavy-particle energy equations can be written as [25]

$$\nabla \cdot \left(\frac{5}{2} k T_\mathrm{e} \boldsymbol{J}_\mathrm{e} + \boldsymbol{h}_\mathrm{e}\right) = -e\boldsymbol{J}_\mathrm{e} \cdot \boldsymbol{E} - \frac{3 n_\mathrm{e} k^2 T_\mathrm{e}}{m_\mathrm{i} n}(T_\mathrm{e} - T_\mathrm{h})\left(\frac{n_\mathrm{a}}{D_\mathrm{ea}} + \frac{n_\mathrm{i}}{D_\mathrm{ei}}\right) - w_\mathrm{e}^{(\mathrm{e})}, \tag{10}$$

$$\nabla \cdot \left(\frac{5}{2} k T_\mathrm{h} \boldsymbol{J}_\mathrm{a} + \frac{5}{2} k T_\mathrm{h} \boldsymbol{J}_\mathrm{i} + \boldsymbol{h}_\mathrm{hp}\right) = e\boldsymbol{J}_\mathrm{i} \cdot \boldsymbol{E} + \frac{3 n_\mathrm{e} k^2 T_\mathrm{e}}{m_\mathrm{i} n}(T_\mathrm{e} - T_\mathrm{h})\left(\frac{n_\mathrm{a}}{D_\mathrm{ea}} + \frac{n_\mathrm{i}}{D_\mathrm{ei}}\right), \tag{11}$$

where $\boldsymbol{h}_\mathrm{e}$ and $\boldsymbol{h}_\mathrm{hp}$ are the densities of heat fluxes transported by the electrons and heavy particles, respectively. The terms with the factor $5/2$ on the left-hand side of each of these equations account for the enthalpy transport by the diffusion fluxes. The first term on the right-hand side accounts for Joule heating of the electron or, respectively, ion species. The second term accounts for the energy exchange between the electrons and the heavy particles due to elastic collisions. The third term on the right-hand side of equation (10) accounts for losses of electron energy due to inelastic collisions and may be written as [27]

$$w_\mathrm{e}^{(\mathrm{e})} = A_\mathrm{i} \omega_\mathrm{e} + w_\mathrm{rad}, \tag{12}$$

where A_i is the energy of ionization of an atom and w_rad designates losses of electron energy through radiation or, in other words, the net emission coefficient (e.g. [28, 29]) integrated over the solid angle.

Adding up equations (10) and (11) gives an equation of conservation of the energy of the plasma as a whole. With the use of equation (1) with $\alpha = \mathrm{e}$ and equation (12), this equation may be written as

$$\nabla \cdot \left[\frac{5}{2} k T_\mathrm{h} \boldsymbol{J}_\mathrm{a} + \frac{5}{2} k T_\mathrm{h} \boldsymbol{J}_\mathrm{i} + \left(\frac{5}{2} k T_\mathrm{e} + A_\mathrm{i}\right)\boldsymbol{J}_\mathrm{e} + \boldsymbol{h}_\mathrm{e} + \boldsymbol{h}_\mathrm{hp}\right] = \boldsymbol{E} \cdot \boldsymbol{j} - w_\mathrm{rad}. \tag{13}$$

Let us multiply equation (4) by $(A_\mathrm{i} - A_\mathrm{f})$, where A_f is the work function of the cathode material. Adding up the obtained equation and equation (13), one obtains another form of the equation of conservation of the plasma energy:

$$\nabla \cdot \left[\frac{5}{2} k T_\mathrm{h} \boldsymbol{J}_\mathrm{a} + \left(\frac{5}{2} k T_\mathrm{h} + A_\mathrm{i} - A_\mathrm{f}\right)\boldsymbol{J}_\mathrm{i} + \left(\frac{5}{2} k T_\mathrm{e} + A_\mathrm{f}\right)\boldsymbol{J}_\mathrm{e} + \boldsymbol{h}_\mathrm{e} + \boldsymbol{h}_\mathrm{hp}\right] = \boldsymbol{E} \cdot j - w_\mathrm{rad}. \tag{14}$$

Equations (13) and (14) represent useful corollaries of equations (10) and (11). Vectors in square brackets on the left-hand sides of equations (13) and (14) represent the density of flux of plasma energy; the non-uniqueness of this quantity originates in the dependence of the flux of energy of a multicomponent reacting mixture on the choice of zeros of enthalpy of elements.

Densities of electron and heavy-particle heat fluxes represent a combination of heat fluxes caused by heat conduction and by the effect inverse to the thermal diffusion and are written as [25]

$$\boldsymbol{h}_\mathrm{e} = -\kappa_\mathrm{e}\nabla T_\mathrm{e} + kT_\mathrm{e}n_\mathrm{e}[A_\mathrm{i}^{(\mathrm{e})}(\boldsymbol{v}_\mathrm{e}-\boldsymbol{v}_\mathrm{i}) + A_\mathrm{a}^{(\mathrm{e})}(\boldsymbol{v}_\mathrm{e}-\boldsymbol{v}_\mathrm{a})], \tag{15}$$

$$\boldsymbol{h}_\mathrm{hp} = -\kappa_\mathrm{hp}\nabla T_\mathrm{h} + kT_\mathrm{h}[n_\mathrm{i}A_\mathrm{i}^{(\mathrm{h})}(\boldsymbol{v}_\mathrm{i}-\boldsymbol{v}_\mathrm{a}) + n_\mathrm{a}A_\mathrm{a}^{(\mathrm{h})}(\boldsymbol{v}_\mathrm{a}-\boldsymbol{v}_\mathrm{i})], \tag{16}$$

where κ_e and κ_hp are thermal conductivities of the electron and heavy-particle gases and $A_\mathrm{i}^{(\mathrm{e})}$, $A_\mathrm{a}^{(\mathrm{e})}$, $A_\mathrm{i}^{(\mathrm{h})}$ and $A_\mathrm{a}^{(\mathrm{h})}$ are kinetic coefficients.

The set of equations also includes the Poisson equation

$$\varepsilon_0\nabla\cdot\boldsymbol{E} = e(n_\mathrm{i}-n_\mathrm{e}). \tag{17}$$

Using this equation, one can rewrite equation (9) as

$$\nabla p = \varepsilon_0(\nabla\cdot\boldsymbol{E})\,\boldsymbol{E}. \tag{18}$$

The primary aim of this work is to study that section of the near-cathode region where the energy flux to the cathode surface is generated. Since the thickness of this section is much smaller than transversal dimensions of the cathode, the density of electric current does not change much here and current transfer across this section of the near-cathode region may be treated as locally planar. It is natural in such a situation to consider a 1D planar model describing a parallel-plane current transfer to a planar cathode through a planar near-cathode region. On the other hand, one can take a step further and consider a 1D spherically symmetric model describing a spherically symmetric current transfer to a hemispherical cathode through a spherically symmetric near-cathode region. As far as a thin near-cathode layer is concerned, the spherically symmetric model will give a solution close to the one given by the planar model; additionally, the spherically symmetric model can provide useful information on physics of the constriction zone, which is an outer part of the near-cathode region where the density of electric current varies between values typical for the arc column and considerably higher values at the cathode surface. In this work, the 1D spherically symmetric model is employed.

Let us designate by r_c the radius of the (hemispherical) cathode, by x distance from the cathode surface measured in the radial direction (so that $r = r_\mathrm{c} + x$ represents the distance from the centre of the cathode), and by J_α, j, E, etc radial components of the corresponding vectors. The above equations are written in the 1D form under the assumption of spherical symmetry, after which equations (3), (4) and (18) may be integrated to give

$$J_\mathrm{i} + J_\mathrm{a} = 0, \tag{19}$$

$$J_\mathrm{i} - J_\mathrm{e} = \frac{j}{e} = -\frac{j_\mathrm{c}}{e}\frac{1}{B}. \tag{20}$$

$$p = p_0 + \varepsilon_0\left(\frac{E^2-E_0^2}{2} - 2\int_x^{r_0-r_\mathrm{c}}\frac{E^2}{r_\mathrm{c}+x}\,\mathrm{d}x\right). \tag{21}$$

Here j_c is a constant having the meaning of the density of electric current coming to the cathode surface from the plasma (a given parameter), $B = (1+x/r_\mathrm{c})^2$, $r = r_0$ is a reference point and E_0 and p_0 are the electric field and the plasma pressure at this point. Equation (19) is written taking into account the fact that the nuclei do not accumulate or disappear at the cathode surface. Note that it is convenient to choose the reference point far away from the cathode, then the second term on the right-hand side of equation (21), while being comparable at high current densities with the first term in the near-cathode space-charge sheath both for a very high-pressure Hg plasma and an atmospheric-pressure Ar plasma, is small outside the sheath, so p_0 may be interpreted as the plasma pressure in the arc chamber. In this work, p_0 is treated as a given parameter.

2.2. Boundary conditions

The system of ordinary differential equations to be solved comprises equation (1) with $\alpha = \mathrm{e}$, equation (5) with $\alpha = \mathrm{i}$, e, energy equations (10) and (11) (any one of these equations may be replaced by equation (13) or equation (14)), equations (15), (16) and (17). These equations are solved in the domain $0 \leqslant x \leqslant L$, where the lower boundary $x = 0$ corresponds to the cathode surface and the upper boundary $x = L$ is placed far enough from the cathode in the constriction zone.

Intuitively, one could expect that altogether eleven boundary conditions must be specified: boundary conditions for density of each species and the electron and heavy-particle temperatures at the cathode surface, similar conditions at $x = L$ and a condition specifying voltage drop applied to the plasma domain under consideration. The latter condition is specified implicitly in terms of the current density at the cathode surface j_c, which is treated as a given parameter. One boundary condition for particle densities at the cathode surface has already been introduced and used: nuclei do not accumulate or disappear there. One more boundary condition for particle densities is specified in terms of pressure p_0, which is treated as a given parameter. Thus, eight more boundary conditions must be specified, and this count conforms to the type of the system of differential equations to be solved, which comprises eight first-order ordinary differential equations.

Let us restrict the consideration with the case where the cathode surface absorbs all the electrons coming from the plasma and reflects none. A boundary condition for the electron density at the cathode surface is written as (e.g. [30])

$$\frac{j_\mathrm{em}}{e} - \frac{n_\mathrm{e}C_\mathrm{e}}{4} = J_\mathrm{e}, \tag{22}$$

where $C_\mathrm{e} = (8kT_\mathrm{e}/\pi m_\mathrm{e})^{1/2}$ is the mean speed of random motion of the electrons. The left-hand side of this boundary

condition represents a difference between the flux of emitted electrons moving from the cathode surface and the flux of plasma electrons moving to the cathode surface due to random motion; the right-hand side represents the net flux of the electrons evaluated in the hydrodynamic approximation. The density j_{em} of electron emission current is evaluated by means of the Richardson or Richardson–Schottky formulas depending on whether the electric field at the cathode surface is directed into the plasma or, respectively, to the cathode.

Let us assume that all the ions coming from the plasma recombine at the cathode surface (and the neutral atoms go back into the plasma). In principle, the boundary condition for the ion density at the cathode surface can be written in a form similar to equation (22) without the first term on the left-hand side. J_{i} at the cathode surface is of the order of $D_{\mathrm{ia}} n_{\mathrm{i}}^{(\mathrm{pl})}/L_{\mathrm{i}}$, where $n_{\mathrm{i}}^{(\mathrm{pl})}$ is a characteristic ion density in the adjacent plasma and L_{i} is a local length scale of variation of parameters of the ion species. It follows from the above-mentioned boundary condition that the ratio of the ion density at the cathode surface to $n_{\mathrm{i}}^{(\mathrm{pl})}$ is of the order of the ratio of the ion mean free path to L_{i}. The latter ratio represents the Knudsen number. Under conditions of applicability of hydrodynamic equations, the Knudsen number must be small and terms of the order of the Knudsen number in hydrodynamic equations are neglected. One should drop such terms also in the boundary conditions in order to be consistent. It follows that the proper boundary condition for the ion density at the cathode surface is vanishing density:

$$n_{\mathrm{i}} = 0. \tag{23}$$

This is the well-known hydrodynamic boundary condition on an absorbing surface, e.g. [31, 32]. A more detailed discussion and further references can be found elsewhere [33].

The heavy-particle temperature at the cathode surface equals T_{w}, the temperature of the surface, which is considered as a given parameter:

$$T_{\mathrm{h}} = T_{\mathrm{w}}. \tag{24}$$

The boundary condition for the electron temperature at the cathode surface is written as

$$\frac{j_{\mathrm{em}}}{e} 2kT_{\mathrm{w}} - \frac{n_{\mathrm{e}} C_{\mathrm{e}}}{4} 2kT_{\mathrm{e}} = J_{\mathrm{e}} \frac{5}{2} kT_{\mathrm{e}} + h_{\mathrm{e}}. \tag{25}$$

The first term on the left-hand side of this boundary condition accounts for the flux of energy transported by (emitted) electrons moving from the cathode surface, evaluated under the conventional approximation of their velocity distribution by the (half-)Maxwellian function with the cathode surface temperature T_{w}, e.g. [3]. (We recall that the average energy per electron equals $2kT_{\mathrm{w}}$ instead of $3kT_{\mathrm{w}}/2$, which is what one could expect intuitively. This is a consequence of the average value of a product being not equal to the product of average values of multipliers; see the Internet site [34] for details.) The second term on the left-hand side of the boundary condition (25) accounts for the flux of energy transported by plasma electrons moving to the cathode surface, and the right-hand side represents the net flux of the electron energy evaluated in the hydrodynamic approximation.

The upper boundary of the calculation domain, $x = L$, is positioned in the constriction zone, where the density of electric current varies between very high values typical of the cathode surface and lower values typical of the arc column. Most models of high-pressure arc discharges are based on the assumption that the arc plasma is in a state of local thermodynamic equilibrium (LTE) except in the vicinity of the electrodes and at the fringes of the arc [29]. As far as the constriction zone is concerned, this assumption is supported by estimates [16], which have been performed for a 30 bar mercury plasma and $j = 10^7\,\mathrm{A\,m^{-2}}$. Furthermore, the estimates [16] showed that the energy balance of the plasma in these conditions is to a first approximation dominated by radiation, meaning that Joule heating of the plasma is approximately balanced by losses of plasma energy through radiation. Therefore, boundary conditions at $x = L$ are formulated in this work assuming that the plasma at $x = L$ is in LTE and its energy balance is dominated by radiation. This assumption will be verified after a solution has been calculated; see section 3.3.

From the mathematical point of view, the proper way to introduce the above-described boundary conditions is to assume that at $x = L$ gradients are negligible so that the balance of particle numbers, momentum and energy is local. In other words, parameters of the plasma at $x = L$ are found by solving (non-differential) equations which follow from equation (1) with $\alpha = \mathrm{e}$, equation (5) with $\alpha = \mathrm{i}, \mathrm{e}$, equations (13), (11) and (17) when the gradient terms are dropped:

$$k_{\mathrm{i}} n_{\mathrm{a}} - k_{\mathrm{r}} n_{\mathrm{i}} n_{\mathrm{e}} = 0, \tag{26}$$

$$n_\alpha e Z_\alpha E - \sum_\beta \frac{n_\alpha n_\beta k T_{\alpha\beta} C_{\alpha\beta}}{n D_{\alpha\beta}} \left(v_\alpha - v_\beta\right) = 0 \quad (\alpha = \mathrm{i}, \mathrm{e}), \tag{27}$$

$$jE = w_{\mathrm{rad}}, \tag{28}$$

$$e J_{\mathrm{i}} E + \frac{3 n_{\mathrm{e}} k^2 T_{\mathrm{e}}}{m_{\mathrm{i}} n} (T_{\mathrm{e}} - T_{\mathrm{h}}) \left(\frac{n_{\mathrm{a}}}{D_{\mathrm{ea}}} + \frac{n_{\mathrm{i}}}{D_{\mathrm{ei}}} \right) = 0, \tag{29}$$

$$n_{\mathrm{i}} = n_{\mathrm{e}}. \tag{30}$$

Equation (26) signifies that ionization is (locally) balanced by recombination. Equations (27) may be interpreted as Ohm's law for the ions and the electrons. Equation (28) signifies that Joule heating of the plasma is balanced by losses of plasma energy through radiation, which are much larger than losses due to heat conduction and due to enthalpy transport by diffusion fluxes; the limiting case of the plasma energy balance dominated by radiation. Equation (29) signifies that Joule heating of the ions is balanced by the energy transferred in elastic collisions to the electron gas. (In fact, the Joule heating of the ions is very small under conditions of interest and the difference $T_{\mathrm{e}} - T_{\mathrm{h}}$ predicted by this equation is negligible; see below.) Equation (30) signifies electrical neutrality of the plasma.

Strictly speaking, equation (26) is not equivalent to the Saha equation, since the ionization rate constant k_{i} in equation (26) depends on n_{e} (due to decay of excited states

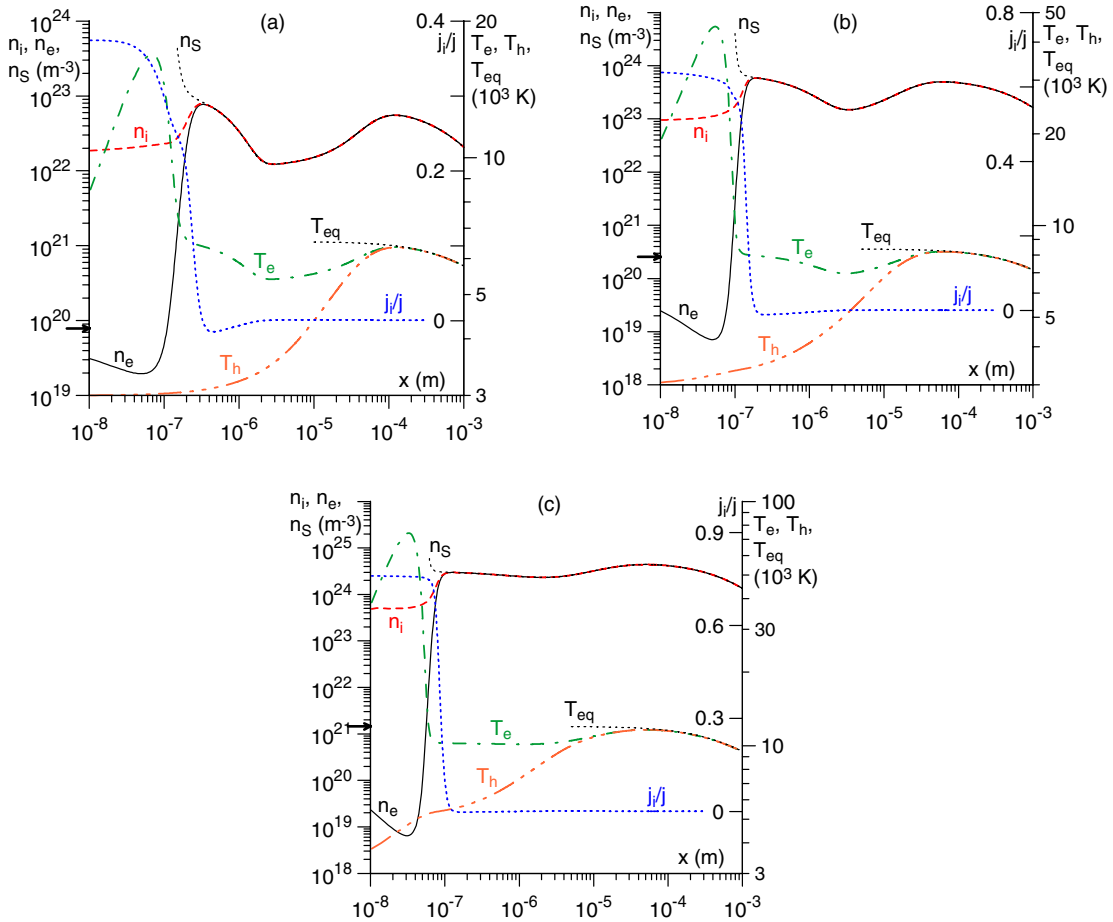

Figure 1. Distributions of parameters in the near-cathode region in mercury at $p_0 = 100$ bar, $T_w = 3000$ K, j_c (A m^{-2}) $= 10^6$ (*a*), 10^7 (*b*), 10^8 (*c*).

due to radiation escape; see appendix A). For given T_e, T_h and p, equation (26) under the assumption $n_i = n_e$ may be written as a cubic equation for n_e. This equation has three real roots, of which only one is positive.

The reference point $r = r_0$ in equation (21) is naturally identified with the upper boundary of the calculation domain, then $p = p_0$ at $x = L$.

Equations (26)–(30) are solved jointly with equations (19) and (20) at given values of $p = p_0$ and $j = j_L$ (here j_L is the local electric current density at $x = L$ which is related to j_c: $j_L = -j_c r_c^2/(r_c + L)^2$). Values of n_i, n_e, T_e and T_h found in this way are used as boundary conditions at the upper boundary of the calculation domain. As mentioned above, the particle densities obtained in this way deviate from those predicted by the Saha equation; we note right now that these deviations are negligible for Hg at all j_c considered and for Ar at high and intermediate j_c; they reach about 100% for Ar at low j_c. The discrepancy between T_h and T_e is negligible (of the order of 10^{-6}) for all conditions treated in this work.

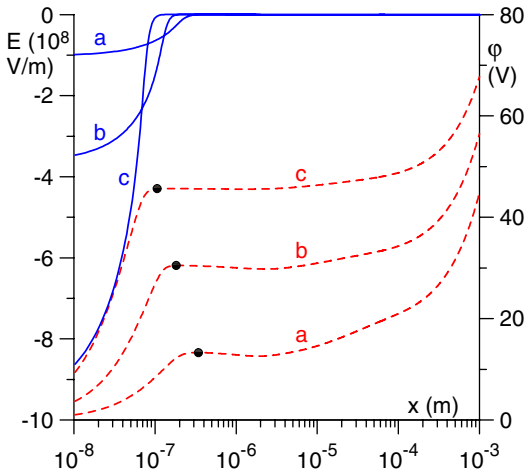

Figure 2. Distributions of electric field and electrostatic potential in the near-cathode region in mercury at $p_0 = 100$ bar, $T_w = 3000$ K. Solid: electric field. Dashed: potential. *a*, *b*, *c*: j_c (A m^{-2}) $= 10^6$, 10^7, 10^8, respectively. Circles: points where separation of charges reaches 1%.

3. Results and discussion

The above-described boundary-value problem (which is quite stiff) is solved numerically as described in appendix B. Results of calculations of the near-cathode region in very high-pressure mercury and atmospheric-pressure argon arcs reported in this work refer to a hemispherical tungsten cathode of radius $r_c = 1$ mm.

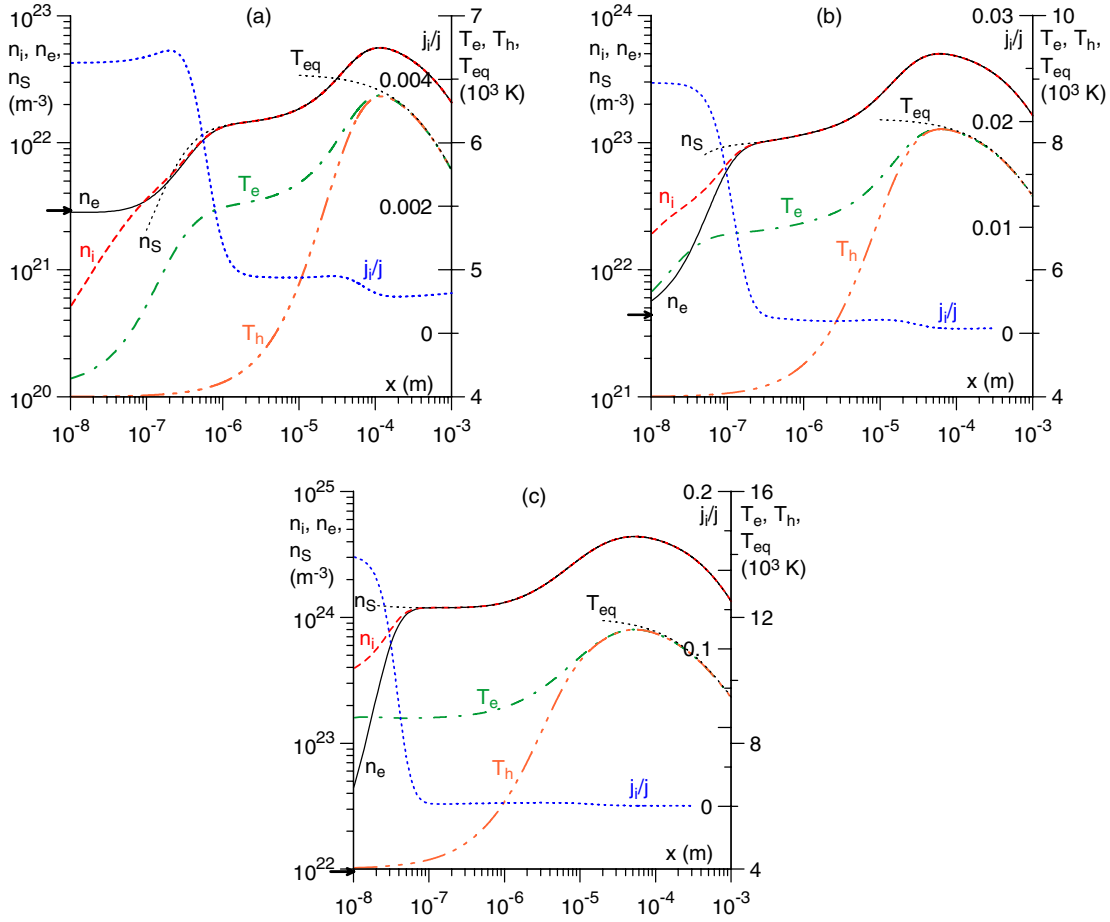

Figure 3. Distributions of parameters in the near-cathode region in mercury at $p_0 = 100$ bar, $T_w = 4000$ K, j_c (A m^{-2}) $= 10^6$ (*a*), 10^7 (*b*), 10^8 (*c*).

3.1. Distributions of plasma parameters in the near-cathode region and current–voltage characteristics (CVCs)

In figures 1–6, distributions of parameters in the near-cathode region are shown for different values of the density j_c of electric current from the plasma to the cathode surface. The parameters shown include densities of the ions and the electrons n_i and n_e, electron and heavy-particle temperatures T_e and T_h, the ion current density $j_i = eJ_i$ normalized by the local electric current density j, the electric field E and electrostatic potential φ. (Zero of potential is chosen at the surface of the cathode.) Arrows on the left of the first y-axis in figures 1, 3 and 5 depict the electron density value $n_{em} = 4j_{em}/eC_e$ which would correspond to equilibrium between electron emission from the cathode surface and the flux of electrons returning to the cathode from the plasma, cf the boundary condition (22). A logarithmic scale in x must be employed in order to obtain informative figures; therefore, the distributions are shown down to a small but non-zero value of x which was chosen taking into account mean free paths and equals 10^{-8} m for Hg and 10^{-7} for Ar.

Another distribution shown in figures 1, 3 and 5 is that of n_S, the charged particle density, evaluated in terms of local heavy-particle and electron temperatures T_h and T_e with $p = p_0$ by means of the Saha equation. Also shown is T_{eq} the plasma temperature which would occur at the same current density in a plasma with a local balance of particle numbers, momentum and energy. (More precisely, equations (26)–(30) jointly with equations (19) and (20) and with equation $p = p_0$, which is used instead of equation (21), are solved at each x with the local

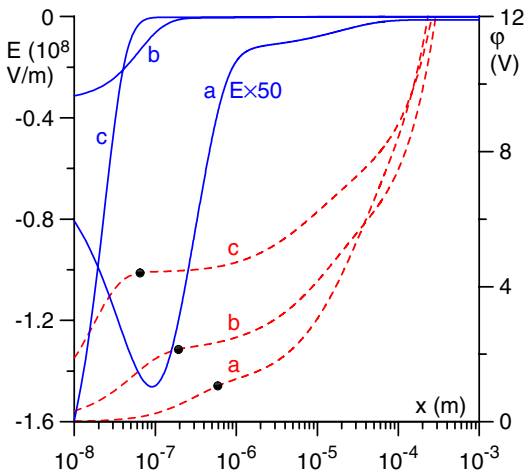

Figure 4. Distributions of electric field and electrostatic potential in the near-cathode region in mercury at $p_0 = 100$ bar, $T_w = 4000$ K. Solid: electric field. Dashed: potential. *a*, *b*, *c*: j_c (A m^{-2}) $= 10^6$, 10^7, 10^8, respectively. Circles: points where separation of charges reaches 1%.

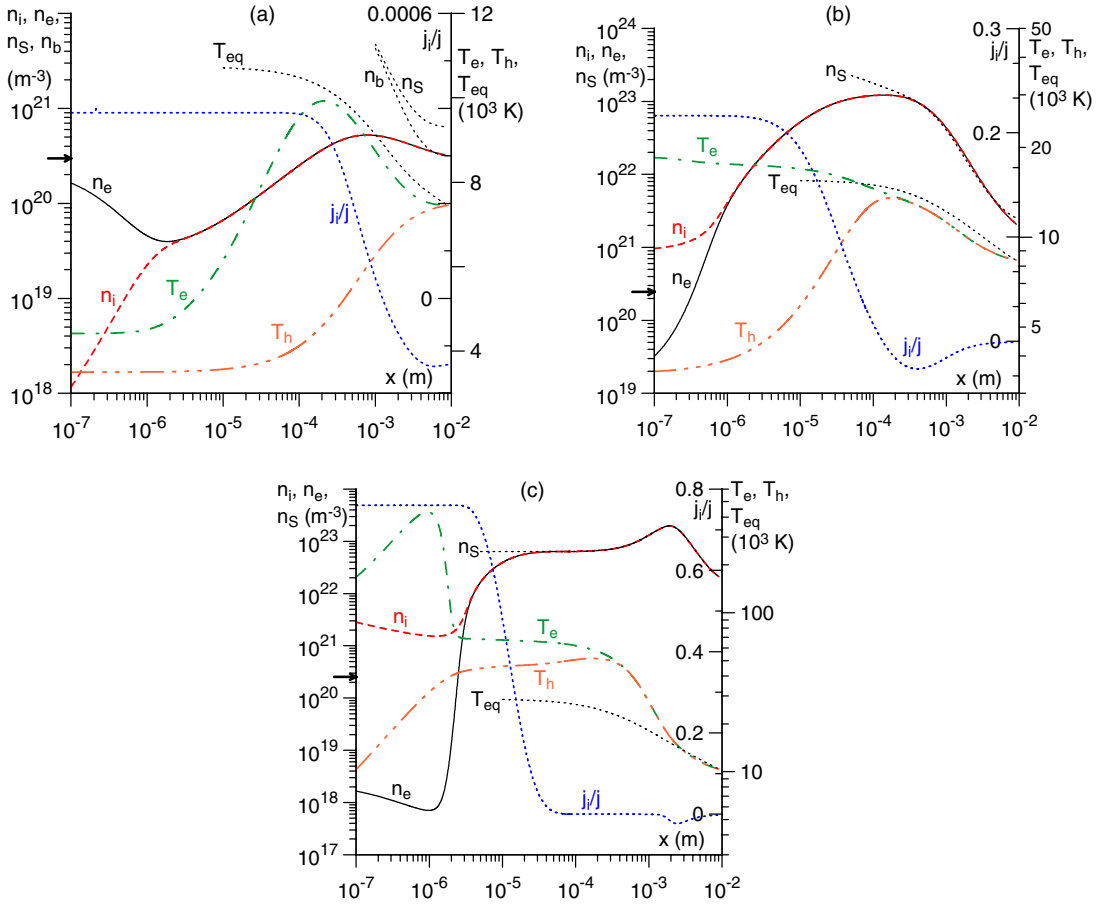

Figure 5. Distributions of parameters in the near-cathode region in argon at $p_0 = 1$ bar, $T_w = 3500$ K, j_c (A m^{-2}) $= 10^6$ (*a*), 10^7 (*b*), 7.8×10^7 (*c*).

value of j. The electron temperature obtained, which virtually coincides with the heavy-particle temperature as mentioned at the end of section 2.2, is designated T_{eq}.) As x decreases, T_{eq} increases, which is a consequence of the increase in the local current density in the direction to the cathode originating in the spherically symmetric geometry being treated. At small distances from the cathode surface, $x \ll r_c$, j becomes virtually constant and so does T_{eq}.

Figures 1–4 refer to mercury plasma at pressure $p_0 = 100$ bar. Figures 1 and 2 refer to the case $T_w = 3000$ K, figures 3 and 4 refer to $T_w = 4000$ K. Consider first the region $x \gtrsim 100\,\mu$m in the case of a low current density at the cathode surface; figures 1(*a*) and 3(*a*). One can see that $n_e \approx n_i$ here, i.e. the plasma is quasi-neutral; $n_e \approx n_S$, i.e. the plasma is in ionization (Saha) equilibrium; $T_e \approx T_h$, i.e. the plasma is in thermal equilibrium. In the framework of the description of the plasma employed in this work, which does not involve the population of excited states, these three kinds of equilibrium jointly amount to the LTE of the plasma. Furthermore, $T_e \approx T_{eq}$ in the region considered, i.e. the energy balance of the plasma is dominated by radiation. In the following, this region will be referred to as a region of radiation-dominated LTE plasma. The plasma temperature and the charged particle density in this region increase with a decrease in x; a consequence of the above-described increase in T_{eq} originating in the geometrical increase in the local current density.

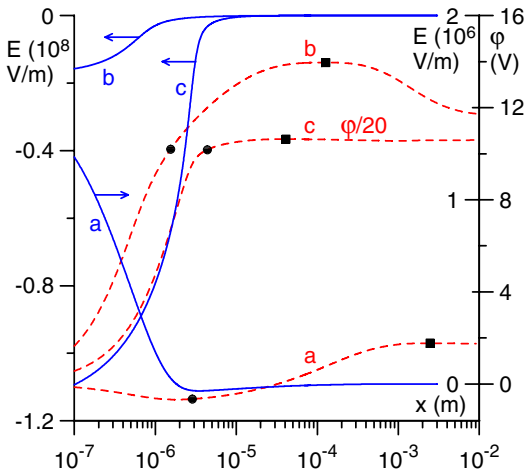

Figure 6. Distributions of electric field and electrostatic potential in the near-cathode region in argon at $p_0 = 1$ bar, $T_w = 3500$ K. Solid: electric field. Dashed: potential. *a*, *b*, *c*: j_c (A m^{-2}) $= 10^6$, 10^7, 7.8×10^7, respectively. Circles: points where separation of charges reaches 1%. Squares: points where the function $\varphi(x)$ attains a maximum value.

A layer separating the region of radiation-dominated LTE plasma from the cathode, in which deviations from LTE and the equilibrium between Joule heating and radiation are localized, will be referred to as a near-cathode non-equilibrium layer. The

thickness of this layer is about 100 μm at low current densities at the cathode surface (figures 1(*a*) and 3(*a*)) and somewhat smaller at higher current densities (figures 1(*b*) and (*c*), 3(*b*) and (*c*)). The latter is due to a higher temperature in the region of the radiation-dominated LTE plasma.

As x decreases and one leaves the region of radiation-dominated LTE plasma and enters the non-equilibrium layer, the equilibrium between Joule heating and radiation losses is the first to break down: while T_{eq} in the non-equilibrium layer weakly increases in the direction of the cathode or is virtually constant, T_e and T_h, still being equal to each other, deviate from T_{eq} in the direction of lower values, i.e. pass through a maximum and then start decreasing: cooling of the plasma by the cathode comes into play. Hence, one can introduce a layer which is adjacent to the region of radiation-dominated LTE plasma and in which the energy balance of the plasma is no longer dominated by radiation, although the plasma is still in LTE. This layer may be called the layer of thermal perturbation.

As x decreases further, T_h rapidly decreases and approaches the temperature of the cathode surface. T_e initially (in the layer of thermal perturbation) decreases jointly with T_h, but very soon deviates from T_h and starts decreasing much more slowly than does T_h. In other words, thermal equilibrium breaks down, and so does LTE on the whole. The ionization equilibrium and quasi-neutrality still prevail. Hence, one can introduce a layer which is adjacent to the layer of thermal perturbation and in which electron and heavy-particle temperatures are no longer equal, although the plasma is still quasi-neutral and ionization equilibrium still holds, a layer of thermal non-equilibrium.

At still smaller x, n_i and n_e deviate from n_S in the direction of lower values: the ionization equilibrium breaks down. Quasi-neutrality breaks down very shortly afterwards, i.e. deviations between n_i and n_e occur and a space-charge sheath is formed. In most cases, the density of ions n_i in the space-charge sheath exceeds the electron density n_e, an exception being the case of a hot cathode and a relatively low current density, which is shown in figure 3(*a*). In the latter case, the space-charge sheath comprises two zones: the outer zone $10^{-7}\,\mathrm{m} \lesssim x \lesssim 10^{-6}\,\mathrm{m}$, where n_i slightly exceeds n_e, and the inner zone $x \lesssim 10^{-7}\,\mathrm{m}$, where n_e exceeds n_i and is approximately equal to n_{em}.

In the cases shown in figure 1, the ion density does not change much in the space-charge sheath except in the vicinity of the sheath edge. It may seem that this behaviour contradicts the boundary condition (23). In fact, there is no contradiction: the computed distributions $n_i(x)$ rapidly decrease down to zero in a very thin layer adjacent to the cathode, which is positioned in the region $x < 10^{-8}\,\mathrm{m}$ and is not shown on the graphs. (This is the so-called ion diffusion layer [31, 33], which is characteristic of the hydrodynamic description of near-cathode layers.)

One can see from figures 2 and 4 that there is a very strong electric field directed to the cathode in the space-charge sheath. The electric field outside the sheath, i.e. in the quasi-neutral plasma, is substantially lower and is not visible on the graph, except in the case of a hot cathode and a low current density represented by the solid line a in figure 4. The electric field in the sheath is non-monotonic in the latter case, which conforms to the above-described variation of sign of the space charge in the sheath occurring in this case. In order to give an idea of an 'edge' of the sheath, points are indicated in figures 2 and 4 where separation of charges reaches 1%. One can see that an increase in the current density results in a decrease of the thickness of the space-charge sheath.

Distributions of the electrostatic potential shown in figures 2 and 4 reveal a more or less pronounced near-cathode voltage drop, which can be identified with the potential difference between the point in the plasma where separation of charges reaches 1% and the cathode surface. (It is not very well pronounced in the case of high T_w and low j_c, which is depicted by line a in figure 4; however it is quite unambiguous if the linear scale in x is used.) As should have been expected, the near-cathode voltage drop decreases with increasing T_w and increases with increasing j_c. The increase in potential in the region $x \gtrsim 10^{-4}\,\mathrm{m}$ is due to resistance of the bulk plasma.

Figures 5 and 6 refer to the argon plasma at pressure $p_0 = 1\,\mathrm{bar}$ and $T_w = 3500\,\mathrm{K}$. In the case of a high current density shown in figure 5(*c*), the near-cathode region has the same structure as that in the case of Hg shown in figures 1 and 3: one can identify the region of radiation-dominated LTE plasma, the layer of thermal perturbation, the layer of thermal non-equilibrium and the space-charge sheath. A difference is that quasi-neutrality of the plasma under conditions of figure 5(*c*) breaks down at considerably smaller x than those at which the ionization equilibrium breaks down, rather than at nearly the same x as is the case for Hg. As a consequence, one can identify one more layer: the one between the layer of thermal non-equilibrium and the space-charge sheath. Here, equilibria of all kinds, including ionization equilibrium, have already broken down, the only exception being the quasi-neutrality of the plasma which still holds. This layer is usually referred to as an ionization layer. Note that such a structure of the near-cathode non-equilibrium layer is similar to the structure of the near-anode perturbation region in high current arcs proposed in [35, 36] . Another difference between the distributions shown in figure 5(*c*) and those depicted in figures 1 and 3 is that T_e and T_h in the layer of thermal perturbation deviate from T_{eq} in the direction of higher values. One more difference is that the thickness of the near-cathode non-equilibrium layer in this case is considerably larger than that under conditions of figures 1–4.

In the case of an intermediate current density, shown in figure 5(*b*), the region of radiation-dominated LTE plasma is not very well pronounced: although the electron and heavy-particle temperatures at $x \gtrsim 10^{-4}\,\mathrm{m}$ are rather close to T_{eq}, there is still a visible difference. While in all the above-discussed cases thermal equilibrium breaks down before (i.e. at larger x) the ionization equilibrium does, it happens the other way round under the conditions of figure 5(*b*). Comparing figures 5(*c*) and (*b*) and also solid lines c and b in figure 6, one can conclude that an increase in the current density under these conditions results in an increase in the thickness of the space-charge sheath, in contrast to what happens under the above-discussed conditions of a very high-pressure Hg plasma.

The case of a relatively low current density is shown in figure 5(*a*). Also plotted in this figure is n_b, the charged

Table 1. Components of the electric current density at the cathode surface, electron temperature at the point of maximum positioned inside the space-charge sheath, fraction of ion current generated outside the near-cathode layer and density of energy flux to the cathode surface.

Figure	j_{iw}/j_c	j_{ew}/j_c	j_{em}/j_c	$j_e^{(cd)}/j_c$	$T_e^{(max)}(10^3\,K)$	$j_{is}j_c/j_sj_{iw}$	q_c (W m^{-2})
1(a)	0.374	0.626	1.313	0.687	16.9	−0.014	1.25×10^7
1(b)	0.640	0.360	0.491	0.131	45.0	0.020	2.32×10^8
1(c)	0.762	0.238	0.281	0.043	74.1	0.070	3.55×10^9
3(a)	0.004	0.996	46.43	45.43	—	0.668	9.22×10^5
3(b)	0.024	0.976	7.716	6.740	—	0.170	-1.18×10^7
3(c)	0.160	0.840	2.033	1.193	—	0.065	-1.07×10^8
5(a)	4×10^{-4}	1.000	4.898	3.898	—	−0.025	-3.67×10^6
5(b)	0.216	0.784	0.824	0.040	18.5	0.011	4.14×10^7
5(c)	0.760	0.240	0.242	0.002	430	0.022	1.29×10^{10}

particle density evaluated in terms of local T_h and T_e with $p = p_0$ under the assumption of local balance of ionization and recombination and quasi-neutrality, i.e. with the use of equations (26) and (30). One can see that there is a visible discrepancy between n_S and n_b in this case; note that n_S coincides with n_b to graphical accuracy in all the other cases. The region of radiation-dominated LTE plasma is absent in this case, the reason being relatively low values of the temperature T_{eq} and, consequently, of the electron density. In fact, quasi-neutrality is the only kind of equilibrium that holds in this case: equalities $T_e = T_{eq}$, $T_h \approx T_e$ and $n_e = n_b$, while being imposed by the boundary conditions at the upper boundary of the calculation domain, $x = 10^{-2}$ m, are violated very close to this boundary. n_e in the space-charge sheath is much higher than n_i, accordingly the electric field in the sheath is directed from the cathode and the sheath voltage is negative.

Distributions of the electrostatic potential in the Ar plasma, shown in figure 6, do not reveal an increase due to a resistance of the bulk plasma which is seen in figures 2 and 4. In fact, in the case of an intermediate current density (line b) a decrease in potential is seen in the range $x \gtrsim 3 \times 10^{-4}$ m. In the case of a high current density (line c) a comparable decrease in potential occurs in the range $x \gtrsim 3 \times 10^{-5}$ m. In both cases, the decrease in potential starts approximately at the edge of the ionization layer. On the other hand, the potential difference in the ionization layer in the case of intermediate current density is comparable to the sheath voltage. Therefore, it seems natural in the case of the atmospheric-pressure argon plasma to define the near-cathode voltage drop as the potential difference between the point in the plasma where the function $\varphi(x)$ attains a maximum value (these points are marked by squares in figure 6) and the cathode surface.

In virtually all the above-described cases, the fraction of current transported by the ions, j_i/j, in the outer section of the near-cathode region is much lower than in the inner section, and the transition from low to higher values occurs in the region where the ionization equilibrium breaks down. The only exception from this pattern occurs under conditions of figure 5(a), where ionization equilibrium does not take place. In some cases, the contribution of the ion current is appreciable in the inner section of the near-cathode region and negligible in the outer section, figures 1, 3(c), 5(b) and (c). In other cases, it is negligible in the inner section of the near-cathode region as well, figures 3(a), (b) and 5(a). It is interesting to note a change in the sign of the ion current that occurs in the case of the Ar plasma at approximately the same point where the charged particle density attains a maximum value.

There are two maxima of the electron temperature for Hg at $T_w = 3000$ K (figure 1), one inside the space-charge sheath and the other in the outer part of the non-equilibrium layer. The first maximum considerably exceeds T_{eq}, the second maximum is close to the local value of T_{eq}. Only the second maximum occurs for Hg at $T_w = 4000$ K (figure 3) and for Ar at a low current density (figure 5(a)). Only the first maximum occurs for Ar at intermediate and high current densities (figures 5(b) and (c)). The physics of the second maximum has already been discussed: the plasma temperature in the region of radiation-dominated LTE plasma increases in the direction of the cathode due to the geometrical increase in the local current density and starts decreasing when cooling of the plasma by the cathode comes into play. The physics of the first maximum is discussed below.

Values of the components of the electric current density at the cathode are given in table 1. Here $j_{iw} = -eJ_i|_{x=0}$ and $j_{ew} = eJ_e|_{x=0}$ are the densities of electric currents transported from the plasma to the cathode surface by the ions and, respectively, electrons; $j_e^{(cd)} = \frac{en_eC_e}{4}|_{x=0}$ is the density of electric current transported by plasma electrons moving to the cathode surface due to random motion. (Obviously, $j_c = j_{iw} + j_{ew}$, $j_{ew} = j_{em} - j_e^{(cd)}$.) Also shown in table 1 is the electron temperature at the first maximum, $T_e^{(max)}$, in cases where this maximum exists.

One can see that in all the cases $j_{ew} > 0$, i.e. the electron emission is sufficient to ensure that the electron flux is directed from the cathode surface into the plasma and not the other way round, cf equation (22). With the increase in j at constant T_w, the fraction of the ion current increases and the fraction of the current of plasma electrons decreases. With the increase in T_w at constant j (for the mercury plasma), the fraction of the ion current decreases and the fraction of the current of plasma electrons increases.

It is convenient to consider the ratio j_{em}/j_c in order to understand the data shown in table 1. Let us first consider cases where this ratio is below unity (cases shown in figures 1(b), (c), 5(b) and (c)). The electron current $j_{ew} = j_{em} - j_e^{(cd)}$ is insufficient to ensure the prescribed current j_c and an appreciable ion current exists. Hence, there is an intensive ionization process in the near-cathode region and there is a substantial supply of energy to the electron gas in the near-cathode region that makes the ionization possible. This energy

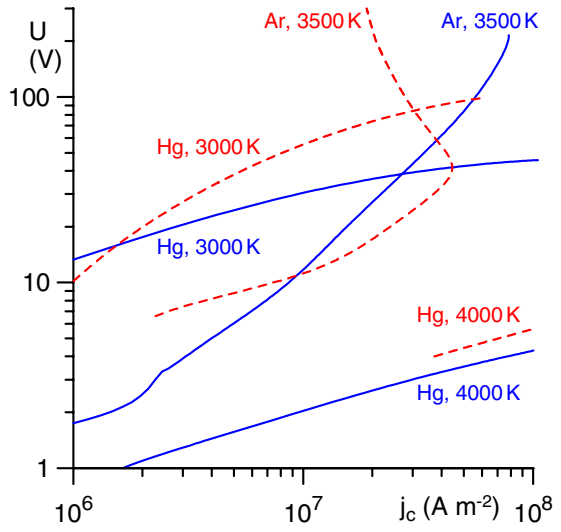

Figure 7. CVCs of the near-cathode layer at a fixed temperature of the cathode surface in mercury at $p_0 = 100$ bar, $T_w = 3000$ and 4000 K, and argon at $p_0 = 1$ bar, $T_w = 3500$ K. Solid: this work. Dashed: the model [3, 44, 45].

supply occurs through acceleration in the space-charge sheath of the electrons emitted by the cathode surface. Hence, the electric field in the sheath is high and very few plasma electrons can overcome it and reach the cathode surface, so $j_e^{(cd)}/j_c \ll 1$.

If j_{em}/j_c exceeds, but is comparable to unity (cases shown in figures 1(*a*) and 3(*c*)), the net electron current is still below j_c, because of the current of plasma electrons, and the ion current is still appreciable. If $j_{em}/j_c \gg 1$ (cases shown in figures 3(*a*), (*b*) and 5(*a*)), the ion current is negligible, $j_{iw}/j_c \ll 1$, and there is a very high current of plasma electrons which virtually compensates j_{em} and thus reduces the net electron current to the prescribed value j_c.

Now the reason for the appearance of the above-described maximum of T_e inside the space-charge sheath is clear: it is a manifestation of a strong supply of energy to the electron gas in the space-charge sheath, which occurs in the cases where j_{em}/j_c is below or slightly above unity and makes possible the generation of an ion current necessary to compensate the deficit of the electron current; the height of this maximum is bigger the lower is ratio j_{em}/j_c.

CVCs of the near-cathode plasma for a fixed temperature of the cathode surface are shown in figure 7; here U is the near-cathode voltage drop defined as described above. All CVCs are monotonically growing. A cusp revealed by the CVC in the case of atmospheric-pressure argon is related to the change in sign of the electric field at the cathode surface, which occurs at $j_c = 2.4 \times 10^6$ A m^{-2} affects the electron emission current. The slope $\mathrm{d}U/\mathrm{d}j_c$ of the CVC in the case of argon starts rapidly increasing as j_c exceeds approximately 7×10^7 A m^{-2}; one can say that CVC approaches ion saturation. This is why the space-charge sheath under conditions of figure 5(*c*) is thicker than that under conditions of figure 5(*b*) and also why the modelling in the case of atmospheric-pressure argon was performed in the range of j_c slightly more narrow than that in the case of mercury (up to 7.8×10^7 A m^{-2} instead of 10^8 A m^{-2}).

3.2. Energy balance of the near-cathode plasma

The most important characteristic to be predicted by a model of the near-cathode plasma region is the density of energy flux coming from the plasma to the cathode surface. A formula governing this quantity in the framework of the hydrodynamic approach being employed in this work is obtained with the use of the expression for the density of plasma energy flux represented by the vector in square brackets on the left-hand side of equation (14) (note that the first and second terms cancel by virtue of equation (19)):

$$q_c = \left[\left(\frac{5}{2} kT_e + A_f \right) (-J_e) - h_e + (A_i - A_f)(-J_i) - h_{hp} \right]_{x=0}. \quad (31)$$

Using boundary conditions (25) and (22), this expression may be rewritten as

$$q_c = -\frac{j_{em}}{e}(A_f + 2kT_w) + \left[\frac{n_e C_e}{4}(A_f + 2kT_e) \right]_{x=0} + (A_i - A_f)[-J_i]_{x=0} + [-h_{hp}]_{x=0}. \quad (32)$$

The first term on the right-hand side describes cooling of the cathode surface by thermionic emission; note that A_f represents the energy necessary to extract an electron from the cathode and $2kT_w$ is the average kinetic energy carried away by an emitted electron. The second term on the right-hand side describes heating of the cathode surface by plasma electrons, evaluated taking into account the energy released at the cathode surface as a result of absorption of electrons. The third term accounts for energy released at the cathode surface as a result of neutralization of ions. The fourth term accounts for energy transported to the cathode surface by heavy-particle heat conduction and the effect inverse to thermal diffusion. Note that equation (32) bears some resemblance to expressions for the energy flux to the cathode employed in simplified models with a collision-free space-charge sheath. For example, one can compare this equation with equation (13) of [3] (Z in the latter equation should be set equal to unity and A_{eff} replaced with A_f): the terms accounting for thermionic cooling and heating by plasma electrons are identical; the term of equation (32) accounting for the energy released at the cathode surface as a result of neutralization of ions is also present in equation (13) of [3]; the difference is that the term accounting for heavy-particle heat conduction is absent from equation (13) of [3] and a term accounting for kinetic energy of incident ions appears instead.

Under condition of practical interest, energy flux from an arc plasma to the surface of a thermionic cathode must be sufficient to heat the surface up to temperatures necessary for sufficiently strong thermionic emission. If the cathode is undoped and there are no additives in the plasma which could contribute to a reduction of the work function through formation of monolayers on the cathode surface, then the temperature of the cathode tip is around 3000 K. Assuming 1000 K for the temperature of the base of the cathode, 10 mm for the cathode height and 100 W m^{-1} K^{-1} for thermal conductivity of cathode material (thermal conductivity of tungsten at 2000 K), one can estimate q_c as 2×10^7 W m^{-2}.

Note that this value refers to the diffuse mode of current transfer; q_c is considerably higher in the spot mode.

Values of q_c calculated for conditions of figures 1–6 are given in table 1. One can see that in the cases shown in figures 3(*b*), (*c*) and 5(*a*) q_c is negative, i.e. the cathode surface is too hot for given values of the current density and thermionic emission cooling outweighs all heating mechanisms. It has been proved that the cathode surface cannot reach temperatures that high [37]. In the case shown in figure 3(*a*) q_c is positive, however by more than an order of magnitude smaller than the above-mentioned value of 2×10^7 W m^{-2}, hence this case is of no practical interest as well. One can conclude that only those cases may be of practical interest in which a strong supply of energy to the electron gas occurs in the space-charge sheath, namely, cases shown in figures 1(*a*)–(*c*), 5(*b*) and (*c*). Only these cases will be considered in the following. Note that the case shown in figure 5(*c*) can hardly be realized since the near-cathode voltage is too high in this case; however this case is maintained under consideration since it is convenient for investigation of trends.

Let us study the balance of energy of electron gas in the near-cathode region under conditions of a strong supply of energy. Integrating equation (10) over the spherical layer comprised between the surface of the cathode and the (spherical) surface $x = \text{const}$, one obtains an equation of integral balance of the energy of electron gas in the layer, which may be written in the form

$$W_c + W_{pl} = W_J - W_{el} - W_i - W_{rad}, \tag{33}$$

$$W_c = -\left[\frac{5}{2}kT_eJ_e + h_e\right]_{x=0}, \qquad W_{pl} = B\left[\frac{5}{2}kT_eJ_e + h_e\right],$$

$$W_J = \int_0^x (-eJ_e)EB\,\mathrm{d}x, \tag{34}$$

$$W_{el} = \int_0^x \frac{3n_ek^2T_e}{m_in}(T_e - T_h)\left(\frac{n_a}{D_{ea}} + \frac{n_i}{D_{ei}}\right)B\,\mathrm{d}x, \tag{35}$$

$$W_i = A_i(BJ_e - J_e|_{x=0}), \qquad W_{rad} = \int_0^x w_{rad}B\,\mathrm{d}x. \tag{36}$$

The physical sense of terms of equation (33) is clear: W_c is the density of energy flux brought by the electrons to the cathode surface; W_{pl} is the energy flux transported by electrons leaving the layer to the outside plasma; W_J is electrical power supplied to the electron gas inside the layer; W_{el}, W_i and W_{rad} are powers lost by the electrons inside the layer in elastic collisions with the heavy particles, in the process of ionization of atoms and through radiation, respectively.

In figure 8 the terms of equation (33) are shown for mercury at $T_w = 3000$ K and $j_c = 10^6$ and 10^8 A m^{-2} and for argon at $j_c = 10^7$ A m^{-2} (i.e. for conditions corresponding to figures 1(*a*), (*c*) and 5(*b*)). One can see that in all the cases $W_c < 0$, i.e. the electron emission is sufficient to ensure that the flux of electron energy is directed from the cathode surface into the plasma and not the other way round, cf equation (25). Close to the cathode, $W_{pl} \approx W_J$: the emitted electrons transport in the direction to the plasma virtually all of the energy they have received from the electric field after leaving the cathode. The energy transported by the electrons is accumulated, i.e. W_{pl} increases with x. Eventually, the ionization losses come into play, then W_{pl} passes through a maximum and starts decreasing.

It is interesting to note that the maximum of the electron temperature T_e inside the space-charge sheath occurs at a smaller distance from the cathode surface than does the maximum of the density W_{pl} of energy flux transported by electrons or, in other words, before the ionization losses come into play in full. The reason is illustrated by figure 9, where functions T_e and W_{pl} are shown jointly with components of the function W_{pl}. Here $h_{ee} = \frac{5}{2}kT_eJ_e$ is the energy flux due to the enthalpy transport by electron current, h_{eT} and h_{ev} designate the first and second terms on the right-hand side of equation (15) and describe electron energy fluxes due to, respectively, heat conduction and the effect inverse to the thermal diffusion. Also shown is the fraction of current transported by the electrons. If enthalpy transport were the dominating mechanism of the electron energy transport, then the points of maximum of T_e and W_{pl} would be close to each other (one can see from figure 9 that variations of J_e are small in this region). In reality, however, a strong heat conduction is present which cools down the electron gas even before the ionization losses come into play in full.

Let us proceed to the energy balance of the plasma on the whole. Integrating equation (14) over the spherical layer comprised between the surface of the cathode and the (spherical) surface $x = \text{const}$ and taking into account equation (19), one obtains an equation of integral balance of the energy of the plasma in the layer, which may be written in the form

$$q_c + q_{pl} = q_J - W_{rad}, \tag{37}$$

where

$$q_{pl} = B\left[\left(\frac{5}{2}kT_e + A_f\right)J_e + (A_i - A_f)J_i + h_e + h_{hp}\right],$$

$$q_J = j_c\varphi. \tag{38}$$

The physical sense of equation (37) is clear: the sum of the energy fluxes from the layer to the cathode surface and to the outside plasma (q_c and q_{pl}, respectively) equals the difference between q_J the electrical power supplied to the layer and W_{rad} the irradiated power. Different versions of this equation have been well known since the work [38]. Relative magnitudes of terms of equation (37) are illustrated by figure 10.

Simplified models of the near-cathode region in high-pressure arc discharges are based on the concept of a near-cathode layer defined as a region that gives dominating contributions to the near-cathode voltage drop and generation of ion current coming to the cathode. It seems natural in the framework of the present (unified) model to identify this layer with the region limited by a point where charge separation amounts to 1%, in the case of the very high-pressure mercury plasma, and a point where the potential distribution attains a maximum value, in the case of the atmospheric-pressure argon. The fraction of the ion current density evaluated at the point defined in such a way, j_{is}/j_s, represents a measure of the ion current generated outside the near-cathode layer, and one should compare this value with the value of the fraction of ion current at the cathode surface, j_{iw}/j_c. The ratio of these

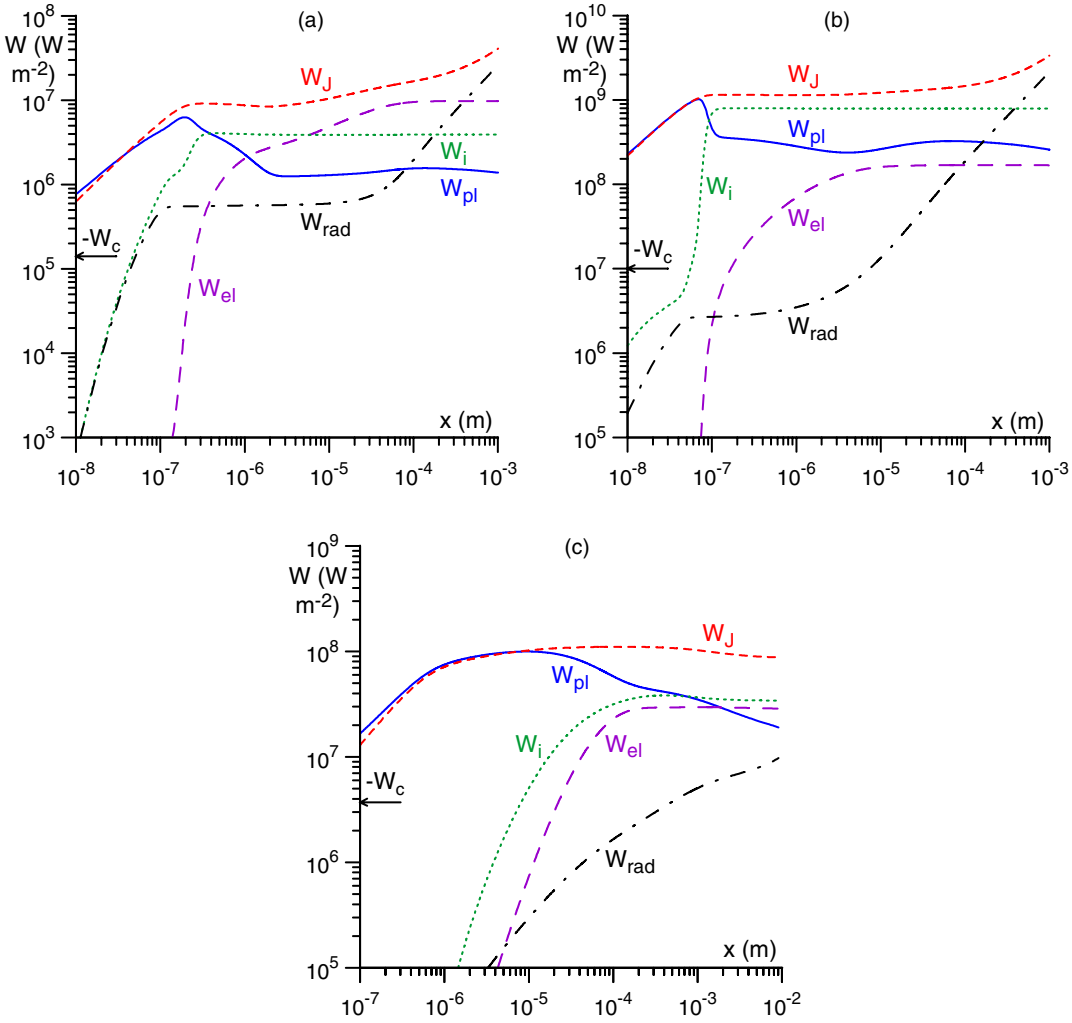

Figure 8. Energy balance of electron gas in the near-cathode region. Mercury, $p_0 = 100$ bar, $T_w = 3000$ K, j_c (A m^{-2}) $= 10^6$ (*a*), 10^8 (*b*); argon, $p_0 = 1$ bar, $T_w = 3500$ K, $j_c = 10^7$ A m^{-2} (*c*).

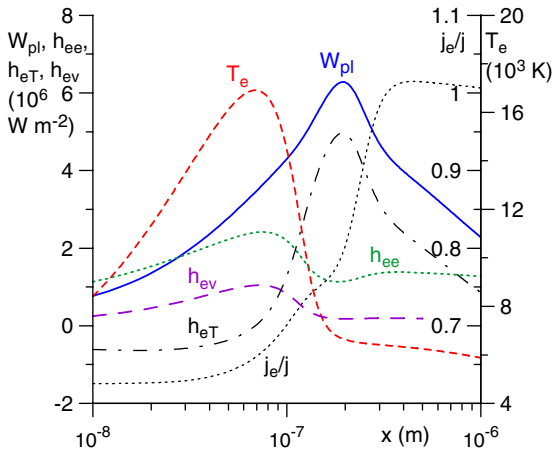

Figure 9. Components of the density of electron energy flux in the near-cathode region. Hg plasma, $p = 100$ bar, $T_w = 3000$ K, $j_c = 10^6$ A m^{-2}.

two values is given in table 1 for conditions of figures 1, 3 and 5. (Since j is nearly constant in the region being considered, this ratio is in fact quite close to j_{is}/j_{iw}.) One can see that this ratio is very small in all the cases of practical interest. Hence, the near-cathode layer defined in this way indeed gives a dominating contribution to the generation of ion current.

Circles and squares in figure 10 designate the position of the edge of the near-cathode layer defined in such a way. In all the cases, radiation losses inside the near-cathode layer play a minor role. q_{pl} at the edge of the layer is very small in the case of mercury at $T_w = 3000$ K and $j_c = 10^6$ A m^{-2} and evidently positive in the other cases. The latter means that it is the near-cathode layer that heats the adjacent plasma in most cases rather than the other way round. This result confirms a similar conclusion derived in [39] for a free-burning arc in atmospheric-pressure argon by means of a model based on a separate treatment of the near-cathode layer and a two-temperature ionization-equilibrium bulk plasma.

3.3. Limitations of the model

The hydrodynamic approach being used in this work is applicable provided that a number of conditions are satisfied. As far as the ions are concerned, the mean free path of collisions between the ions and the atoms, λ_{ia}, should be much smaller than the local length scale L_i of variation of parameters of the

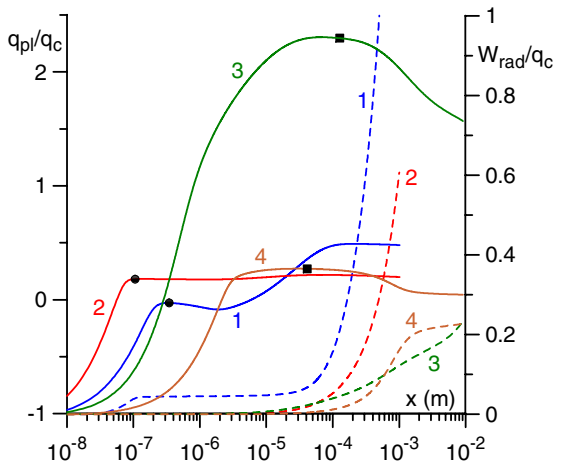

Figure 10. Energy balance of the near-cathode plasma. Solid: $q_{\rm pl}/q_{\rm c}$. Dashed: $W_{\rm rad}/q_{\rm c}$. Circles, squares: edge of the near-cathode layer. Mercury, $p_0 = 100$ bar, $T_{\rm w} = 3000$ K, $j_{\rm c}$ (A m^{-2}) $= 10^6$ (1), 10^8 (2); argon, $p_0 = 1$ bar, $T_{\rm w} = 3500$ K, $j_{\rm c}$ (A m^{-2}) $= 10^7$ (3), 7.8×10^7 (4).

ion species; work of the electric field over the ion mean free path should be considerably smaller than the thermal energy of the neutral atoms:

$$\lambda_{\rm ia} \ll L_{\rm i}, \qquad e|E|\lambda_{\rm ia} \ll kT_{\rm h}. \tag{39}$$

As far as the electrons are concerned, the length of Maxwellization of electrons, $\lambda_{\rm m}$, should be much smaller than the local length scale $L_{\rm e}$ of the variation of the parameters of the electron species; the ratio of average frequencies of momentum transfer in electron–electron and electron–atom collisions should be much larger than the particle mass ratio:

$$\lambda_{\rm m} \ll L_{\rm e}, \qquad \bar{\nu}_{\rm ee}/\bar{\nu}_{\rm ea} \gg m_{\rm e}/m_{\rm a}. \tag{40}$$

Note that $\bar{\nu}_{\rm ee} = n_{\rm e}C_{\rm e}\bar{Q}_{\rm ee}^{(1,1)}$ and $\bar{\nu}_{\rm ea} = n_{\rm a}C_{\rm e}\bar{Q}_{\rm ea}^{(1,1)}$; here and further $\bar{Q}_{\alpha\beta}^{(1,1)}$ designate the energy-averaged cross sections for momentum transfer evaluated as described in appendix A.

The mean free path for collisions between ions and atoms is defined as $\lambda_{\rm ia} = 1/(n_{\rm i}{+}n_{\rm a})\bar{Q}_{\rm ia}^{(1,1)}$. (For low ionization degree $\lambda_{\rm ia}$ coincides with the conventional mean free path of ions in the gas of atoms, while for a plasma close to full ionization $\lambda_{\rm ia}$ represents the mean free path of atoms in the ion gas.) The length of Maxwellization is defined as (see appendix C of [40])

$$\lambda_{\rm m} = \frac{1}{\sqrt{n_{\rm e}\bar{Q}_{\rm ee}^{(1,1)}(n_{\rm e}\bar{Q}_{\rm ee}^{(1,1)} + n_{\rm a}\bar{Q}_{\rm ea}^{(1,1)})}}. \tag{41}$$

The local length scales of variation of parameters of the ion and electron species are defined as

$$L_{\rm i} = n_{\rm i}\left|\frac{{\rm d}n_{\rm i}}{{\rm d}x}\right|^{-1}, \qquad L_{\rm e} = n_{\rm e}\left|\frac{{\rm d}n_{\rm e}}{{\rm d}x}\right|^{-1}. \tag{42}$$

Distributions of the above-described length scales in the near-cathode layer are shown in figure 11. Singularities of the dependences $L_{\rm i}(x)$ and $L_{\rm e}(x)$ at the extreme points of functions $n_{\rm i}(x)$ and, respectively, $n_{\rm e}(x)$ are of no interest in the present context and should be disregarded. The edge of the space-charge sheath in figure 11 is conveniently indicated by a merger of the curves $L_{\rm i}$ and $L_{\rm e}$; the region where the ion current is generated may be identified with the use of the ratio $j_{\rm i}/j$ which for convenience is added to this figure.

In the case of a very high-pressure mercury plasma (figures 11(*a*) and (*b*)), $L_{\rm i}$ exceeds $\lambda_{\rm ia}$ by at least an order of magnitude throughout the whole near-cathode region. In the case of an atmospheric-pressure argon plasma at the intermediate current density (figure 11(*c*)), $L_{\rm i}$ exceeds or considerably exceeds $\lambda_{\rm ia}$ in most of the near-cathode region, an exception being a narrow region in the vicinity of the sheath edge where the two lengths are close. At the high current density (figure 11(*d*)), $L_{\rm i}$ is below $\lambda_{\rm ia}$ in the space-charge sheath and in the inner part of the ionization layer.

Distributions of the ratio $e|E|\lambda_{\rm ia}/kT_{\rm h}$ (which are skipped for brevity) are as follows. In the case of a very high-pressure mercury plasma, this ratio is of order 10^{-4}–10^{-2} in the quasi-neutral plasma and reaches values of order unity in the space-charge sheath. In the case of an atmospheric-pressure argon plasma at the intermediate current density, this ratio is of order 10^{-3}–10^{-1} in the quasi-neutral plasma and reaches values of order 10 in the space-charge sheath. It follows that the assumption of the ion distribution function being close to a Maxwellian function with a temperature equal to that of neutral atoms is justified in the quasi-neutral plasma but not in the sheath. Results of the present calculations that are skipped for brevity show that the dominating mechanism of ion transport in the sheath is drift in the sheath electric field; diffusion is a minor effect. Hence, the mobility of the ions is the only relevant transport coefficient of the ions. Since the frequency of collisions of (singly charged) ions with atoms of a parent gas depends on the collision energy rather weakly, the dependence of the ion mobility on the shape of the ion distribution function is rather weak as well. Therefore, deviations of the ion distribution from a Maxwellian function with a temperature equal to that of neutral atoms, which are likely to occur in the sheath, should not cause an appreciable error in the above-described cases. This reasoning does not apply in the case of an atmospheric-pressure argon plasma at high current densities: $e|E|\lambda_{\rm ia}/kT_{\rm h}$ in this case is of order of 10^{-3}–10^{-2} outside the ionization layer, becomes comparable to unity in the ionization layer and reaches values of the order of 10^2 inside the sheath; hence deviations of the ion distribution from a Maxwellian function with a temperature equal to that of neutral atoms are not confined to the sheath but occur in the ionization layer as well.

One can conclude that in the case of a very high-pressure mercury plasma the hydrodynamic (diffusion) description of motion of the ions, used in this work, is reasonably well justified in the whole near-cathode region, including the space-charge sheath. This description remains reasonably well justified in the case of an atmospheric-pressure argon plasma at the intermediate current density, but not at the high current density. A further discussion of this point is given in the next section.

In the case of a very high-pressure mercury plasma (figures 11(*a*) and (*b*)), the electron Maxwellization length $\lambda_{\rm m}$

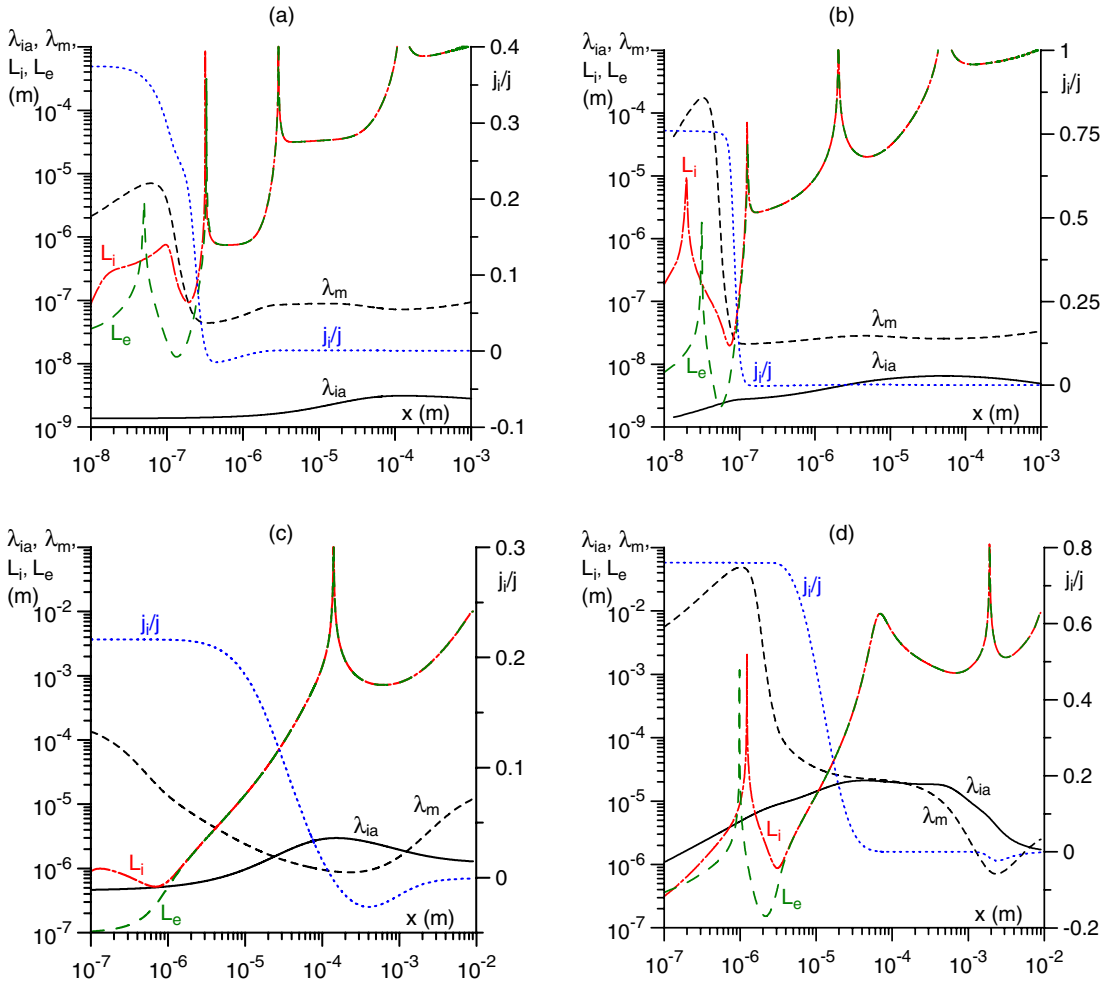

Figure 11. Mean free path of collisions between the ions and the atoms, length of Maxwellization of electrons and local length scales of variation of parameters of the ion and electron species. Mercury, $p_0 = 100$ bar, $T_w = 3000$ K, j_c (A m^{-2}) $= 10^6$ (*a*), 10^8 (*b*); argon, $p_0 = 1$ bar, $T_w = 3500$ K, j_c (A m^{-2}) $= 10^7$ (*c*), 7.8×10^7 (*d*).

considerably exceeds L_e in the bulk of the space-charge sheath. It follows that in the bulk of the sheath the electron distribution function may substantially deviate from the Maxwellian one and the approach to the calculation of the electron transport employed in this work becomes unjustified. One can hope, however, that this does not cause an appreciable error since electron transport in the bulk of the sheath amounts to a trivial acceleration of emitted electrons by the sheath electric field, and the latter is induced mostly by the ions since $n_e \ll n_i$ in the bulk of the sheath. This reasoning does not apply in the vicinity of the sheath edge and in the quasi-neutral plasma, where ionization comes into play. However, λ_m here is comparable to, or considerably smaller than, L_e, so one can hope that the approach being used is at least qualitatively correct. The situation is similar in the case of an atmospheric-pressure argon plasma at the intermediate current density: $\lambda_m \gg L_e$ in the sheath, however $\lambda_m \lesssim L_e$ in the ionization layer. The least favorable situation again occurs in the case of an atmospheric-pressure argon plasma at the high current density, where $\lambda_m \gg L_e$ both in the sheath and in a substantial part of the ionization layer, hence the approach being used can be at best qualitatively correct.

Distributions of the ratio $\bar{\nu}_{ee}/\bar{\nu}_{ea}$ (which are skipped for brevity) are as follows. In the case of a very high-pressure mercury plasma, $\bar{\nu}_{ee}/\bar{\nu}_{ea}$ is comparable to m_e/m_a in the inner section of the space-charge sheath and considerably exceeds m_e/m_a in the vicinity of the sheath edge and in the quasi-neutral plasma. In the case of an atmospheric-pressure argon plasma, $\bar{\nu}_{ee}/\bar{\nu}_{ea}$ is much higher than m_e/m_a in the whole near-cathode region at the intermediate current density. At the high current density, $\bar{\nu}_{ee}/\bar{\nu}_{ea}$ is much smaller than m_e/m_a in the inner section of the space-charge sheath and much higher than m_e/m_a in the vicinity of the sheath edge and in the quasi-neutral plasma, including in the ionization layer. Thus, the second inequality in (40) is less restrictive than the first one and does not affect the above conclusions on the validity of the hydrodynamic approach used in this work.

The boundary conditions imposed at $x = L$, equations (26)–(30), are applicable provided that LTE and the local balance between Joule heating and radiation losses do occur in the near-cathode plasma and occur at distances from the cathode small enough for the current transfer to be locally 1D and convective effects negligible. This is the case for a very high-pressure mercury plasma, where the

thickness of the near-cathode non-equilibrium layer, which separates the region of radiation-dominated LTE plasma from the cathode, is about 100 μm or even smaller. The thickness of the near-cathode non-equilibrium layer in an atmospheric-pressure argon plasma at the high current density is about 3 mm; the approximation of locally 1D current transfer in a quiescent plasma usually loses its validity at distances from the cathode surface smaller than that. At the intermediate current density, the region of radiation-dominated LTE plasma is not very well pronounced. There is no equilibrium of any kind except for quasi-neutrality in the near-cathode region at the low current density.

Thus, the assumption that the plasma at the upper boundary of the calculation domain is in LTE and its energy balance is dominated by radiation is justified in the case of a very high-pressure mercury plasma but not in the case of an atmospheric-pressure argon plasma. On the other hand, the plasma–cathode interaction on the whole is governed by the above-mentioned near-cathode layer which gives dominating contributions to the near-cathode voltage drop and generation of ion current to the cathode. This layer has a thickness of order of 100 μm in the case of an atmospheric-pressure argon plasma, and it is this layer that heats the adjacent plasma rather than the other way around. Dependence of this layer on what happens on scales of the order of 1 mm or larger is weak; hence inaccurate boundary conditions at the upper boundary of the calculation domain can hardly spoil a solution in this layer. Therefore, one can hope that the present model in the case of an atmospheric-pressure argon plasma represents a reasonable approximation in the near-cathode layer which governs the plasma–cathode interaction as a whole, although not on larger length scales.

Only singly charged ions are taken into account in the model considered. LTE calculations of partial composition of a 100 bar Hg plasma and a 1 bar Ar plasma in the temperature range of up to 20×10^3 K show that the fraction of doubly charged ions does not exceed approximately 1%, so the presence of multiply charged ions can be safely neglected at T_e below 20×10^3 K. In the present simulations, the maximum value of T_e in the near-cathode region occurs inside the space-charge sheath under conditions of practical interest (figures 1(*a*)–(*c*), 5(*b*) and (*c*)). However, the formation of multiple ions is governed not by this value (the local value of n_e is very small), but rather by values of T_e in the region where the ion flux to the cathode is generated. There is only one case in which the latter values exceed 20×10^3 K, that of an atmospheric-pressure argon plasma and a high current density, shown in figure 5(*c*): T_e in the ionization layer is about 70×10^3 K in this case. We recall that the case shown in figure 5(*c*) can hardly be realized since the near-cathode voltage is too high, so the latter value is probably exaggerated. Nevertheless, one cannot exclude the possibility of T_e in the ionization layer of an atmospheric-pressure argon arc exceeding 20×10^3 K.

The latter does not automatically mean that multiply charged ions are formed under non-LTE conditions of this work: the second and higher ionizations must occur sufficiently fast for this to happen. Formation of doubly and triply charged ions in the ionization layer in an atmospheric-pressure argon arc was studied numerically in [6] under the assumption that the electron temperature is constant across the ionization layer for T_e of up to 50×10^3 K and the current density of 10^8 A m^{-2}. It was found that the ion current to the cathode is formed in an inner section of the ionization layer where the singly charged ions are dominant, the latter being a consequence of a successive decrease in rate constants of each subsequent ionization. Therefore, the ion current can be calculated accurately enough neglecting the presence of multiply charged ions, which justifies the neglect of formation of doubly and triply charged ions also in this work.

Only atomic ions are taken into account in the model considered. In reality molecular ions may also be present, which are formed through the conversion reaction

$$M^+ + 2M \rightarrow M_2^+ + M, \tag{43}$$

where M is Ar or Hg atom. The presence of molecular ions slightly changes the equilibrium electron density at given p, T_e, and T_h. However, much more essential may be the effect of molecular ions on parameters in the region where the ion flux to the cathode is generated, because the rate of recombination of these ions with electrons may exceed substantially that of atomic ions. The effect of molecular ions may be neglected if the rate of their recombination with electrons is much smaller than the ionization rate. An upper estimate of the recombination rate for molecular ions is given by the conversion rate; hence a sufficient condition allowing one to neglect the effect of molecular ions reads $k_c n_a^2 n_i \ll k_i n_a n_e$, where k_c is the conversion rate constant. Assuming that the densities of electrons and ions are comparable, one can rewrite the latter inequality as

$$k_c n_a \ll k_i. \tag{44}$$

Using the low-temperature values of the conversion rate constants for Ar [41] and Hg [42] and assuming that k_c varies with T_h proportionally to $T_h^{-3/4}$ [43], one finds that for typical T_h values about 3000 K the condition (44) is fulfilled if the electron temperature in the region where the ion flux is generated exceeds approximately 7×10^3 K for Hg at 100 bar and 12×10^3 K for Ar at 1 bar. One can see from figures 1 and 5 that inequality (44) is valid for mercury and argon at the intermediate and high current densities. For mercury at $j_c = 10^6$ A m^{-2} this inequality does not hold and a more careful study is required; we recall that this inequality is not a necessary condition but only sufficient.

3.4. Validity of simplified models

3.4.1. Analysis of physical bases of simplified models. Once dominating physical mechanisms have been identified, one can analyse physical bases of simplified models of the near-cathode region in high-pressure arc discharges (which are many; see review [16] and references therein). The first conclusion concerns the role of the near-cathode space-charge sheath. The above-described numerical results have shown that there is an intensive ionization process in the near-cathode layer and the

supply of energy to the electron gas that makes the ionization possible occurs through acceleration of the emitted electrons in the space-charge sheath. Regimes in which the sheath plays a minor role are in principle possible; however, they do not occur under conditions of high-pressure arc discharges. Thus, the space-charge sheath is of primary importance and models of plasma–cathode interaction in high-pressure arc discharges which neglect the sheath cannot be considered as physically relevant.

Simplified models used in most works (for example [3, 44, 45], [9] and [11]) employ the assumption of a collision-free motion of the ions across the space-charge sheath. If the collisions are rare, the average number of collisions suffered by an ion while travelling over a distance $\mathrm{d}x$ is $\mathrm{d}x/\lambda_{\mathrm{ia}}$. (Note that the biggest value of the ionization degree of plasma in the space-charge sheath under conditions of figures 1, 3 and 5 occurs at the sheath edge under conditions of figure 5(*c*) and is about 0.1. In other words, the ionization degree of the plasma inside the sheath is small in all cases and the length λ_{ia} defined in section 3.3 represents the mean free path of an ion in the gas of atoms.) If the collisions are frequent and the ions perform a random walk rather than a rectilinear motion, then the average number of collisions is $\bar{\nu}_{\mathrm{ia}}\,\mathrm{d}x/|v_{\mathrm{i}}|$, where v_{i} is the local ion diffusion velocity (so that $\mathrm{d}x/|v_{\mathrm{i}}|$ represents the time of diffusion of an ion over the distance $\mathrm{d}x$) and $\bar{\nu}_{\mathrm{ia}} = n_{\mathrm{a}}(8kT_{\mathrm{h}}/\pi m_{\mathrm{ia}})^{1/2}\bar{Q}_{\mathrm{ia}}^{(1,1)}$ is the local average frequency of momentum transfer in ion–atom collisions. A uniformly valid estimate may be obtained by adding up the two expressions given above. Thus, the average number of collisions suffered by an ion while crossing the space-charge sheath is estimated by integrating $\lambda_{\mathrm{ia}}^{-1} + \bar{\nu}_{\mathrm{ia}}\,|v_{\mathrm{i}}|^{-1}$ over the sheath. (We recall that the sheath is identified with a region where the charge separation exceeds 1% in the framework of this model.) Values of this integral for conditions of figures 1(*a*)–(*c*), 5(*b*) and (*c*) are 1.4×10^4, 4.7×10^3 , 4×10^2, 4.5 and 0.97, respectively. One can conclude that in the case of a very high-pressure mercury plasma the assumption of a collision-free motion of the ions across the space-charge sheath is definitely unjustified.

Strictly speaking, this assumption is unjustified in the case of an atmospheric-pressure argon plasma as well, since the average number of ion collisions is comparable to unity rather than small. On the other hand, the only parameter contributed by a sheath model to the overall evaluation scheme of the approaches [3, 44, 45], [9] and [11] is the electric field at the cathode surface, which affects the electron emission current through the Schottky correction, and one can show similarly to [46] that surface electric fields calculated in the framework of models of collision-free and collision-dominated sheaths are not very different under conditions where the number of collisions is of the order unity. Besides, the dependence of the Schottky correction on the surface electric field is not very strong (square-root). As a consequence, the difference between values of the Schottky correction obtained with the use of the two models is typically below 0.1 eV. In other words, the collision-free and collision-dominated sheath models give similar results in the intermediate case where the number of ion collisions in the sheath is of the order unity, and this allows one to assume that both results are realistic. Thus, both the simplified approaches [3, 44, 45], [9] and [11] and the model of this work give a realistic description of the space-charge sheath in an atmospheric-pressure argon plasma.

The models [3, 44, 45], [9] and [11] comprise separate treatments of a quasi-neutral ionization layer and a space-charge sheath with frozen ionization and recombination. Results of this work show that this approximation is reasonable for an atmospheric-pressure argon plasma but not for a very high-pressure mercury plasma: while variations of j_{i}/j under conditions of figure 5 clearly occur outside the space-charge sheath, these variations occur virtually simultaneously with the violation of quasi-neutrality under conditions of figure 1.

The electron temperature in the ionization layer is treated in [3, 44, 45], [9] and [11] as constant (and is governed by an equation of integral balance). Results of this work show that this approximation is reasonable for an atmospheric-pressure argon plasma: T_{e} varies in the ionization layer from 17.5×10^3 to 15.4×10^3 K and from 68.2×10^3 to 67.6×10^3 K under conditions of figures 5(*b*) and (*c*), respectively, i.e. rather weakly. (In the framework of the present model, the ionization layer is identified with a region confined by the sheath edge, i.e. a point where the charge separation exceeds 1% and a point where deviation of n_{e} from n_{S} reaches 50%.)

It was shown in the preceding section that λ_{ia} exceeds L_{i} in a substantial part of the ionization layer in an atmospheric-pressure argon plasma at high current density or, equivalently, a high near-cathode voltage U. The coupling between the ions and the atoms is not strong enough under such conditions and the conventional hydrodynamic, or diffusion, description of motion of the ions in the ionization layer loses its validity. This conclusion confirms the reasoning of the model [3, 44, 45], in which the ionization layer is described by means of the multifluid theory [5] that also takes into account, in addition to the effects accounted for by the diffusion theory, inertia of the ions and the atoms and momentum exchange between the ions and the atoms due to volume reactions. A solution for the ionization layer in atmospheric-pressure arcs in inert gases at high near-cathode voltages obtained in this way is physically reasonable and substantially different from that given by the diffusion theory; see discussion in [16]. The model [11] also employs the multifluid theory for the ionization layer, although in a somewhat reduced form; see [16] for a further discussion. One should assume therefore that the model [3, 44, 45] and maybe also the model [11] are better justified in the case of atmospheric-pressure arcs in argon at high U than the present model.

The conclusion is that the simplified models [3, 44, 45], [9] and [11] are unjustified in the case of very high-pressure mercury plasma. The simplified models are reasonably well justified in the case of atmospheric-pressure argon plasma at moderate U and some of these models also at high U.

3.4.2. Comparison of results. A comparison of CVCs of the near-cathode layer for a fixed temperature of the cathode surface given by the present model with those given by the simplified model [3, 44, 45] is shown in figure 7. The model

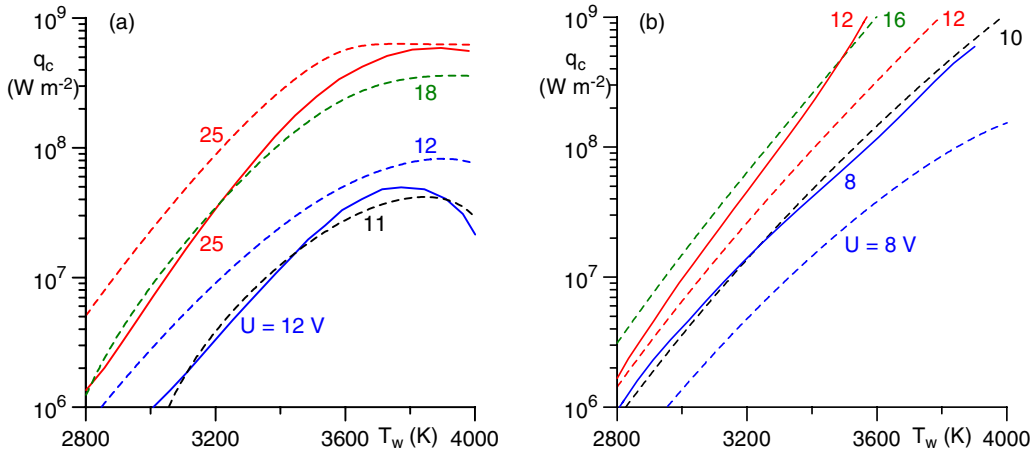

Figure 12. The density of energy flux to the cathode surface versus the cathode temperature at fixed near-cathode voltage drop. Solid: this work. Dashed: the model [3, 44, 45]; (*a*) argon, $p_0 = 1$ bar; (*b*) mercury, $p_0 = 100$ bar.

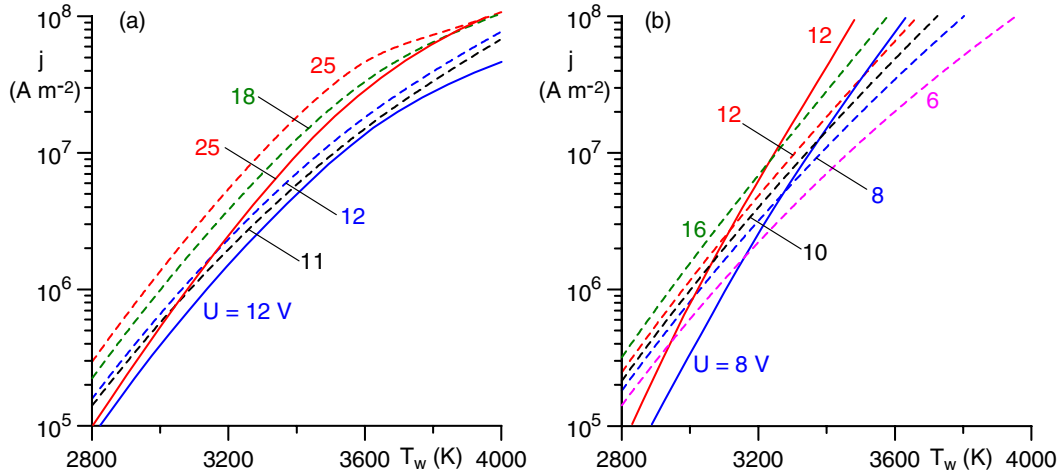

Figure 13. The electric current density at the cathode versus the cathode temperature at fixed near-cathode voltage drop. Solid: this work. Dashed: the model [3, 44, 45]; (*a*) argon, $p_0 = 1$ bar; (*b*) mercury, $p_0 = 100$ bar.

[3, 44, 45] assumes U as a control parameter (and not j_c as does the model of this work.) Being destined for the near-cathode layer, the model [3, 44, 45] breaks down if U is too low. In the case of mercury at $T_w = 4000$ K, the breakdown occurs at $U = 4.0$ V, which limits the range of existence of solution to $j_c \geqslant 3.7 \times 10^7$ A m^2. In the case of argon, the breakdown occurs at $U = 6.6$ V, which limits the range of existence of solution to $j_c \geqslant 2.3 \times 10^6$ A m^2. In the case of mercury at $T_w = 3000$ K, difficulties related to multiplicity of roots (see [16]) appear at $U > 99$ V, which limits the range of existence of solution to $j_c \leqslant 6.1 \times 10^7$ A m^{-2}. In the case of argon, the dependence $j_c(U)$ is non-monotonic, due to inertia of the ions and the atoms in the ionization layer and the momentum exchange between the ions and the atoms due to volume reactions. (We recall that these effects are not described by the diffusion equations used in this work but are taken into account in the multifluid theory employed in the model [3, 44, 45].)

Figure 7 conveniently illustrates the range of existence of solution in the framework of the simplified model [3, 44, 45] and also general trends exhibited by this solution, which are similar to the ones displayed by the model of this work except for the above-mentioned non-monotony of the dependence $j_c(U)$. However, what is needed for the calculation of plasma–cathode interaction in arc discharges is not CVCs at a fixed temperature of the cathode surface but rather dependences of the densities of energy flux and electric current to the cathode surface on the local surface temperature at a fixed near-cathode voltage drop; see [16] and references therein. These dependences predicted by the model of this work and the simplified model [3, 44, 45] are shown in figures 12 and 13. Again, there is qualitative agreement between the solutions given by the present model and the simplified model [3, 44, 45]. In particular, the present model gives a non-monotonic dependence $q_c(T_w)$ in the case of atmospheric-pressure argon (figure 12(*a*)), which is well known from simplified models and represents the root reason for the existence of multiple modes of current transfer to thermionic cathodes (see [16] and references therein). In the case of an atmospheric-pressure argon plasma at moderate U, the agreement between the two models is not only qualitative but also quantitative: the simplified solution for $U = 11$ V is close

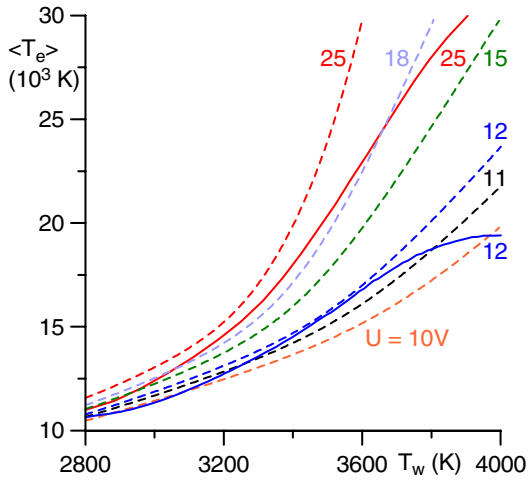

Figure 14. The average electron temperature in the ionization layer versus the cathode temperature at fixed near-cathode voltage drop. Argon, $p_0 = 1$ bar. Solid: this work. Dashed: the model [3, 44, 45].

to the solution given by the present model for $U = 12$ V in the whole range of T_w considered.

Solid lines in figure 14 depict an average value of the electron temperature in the ionization layer evaluated by means of numerical results of this work as $\langle T_e \rangle = (T_e^{(1)} + T_e^{(2)})/2$, where $T_e^{(1)}$ and $T_e^{(2)}$ are values of the electron temperature at the edge of the space-sheath and, respectively, at the edge of the ionization layer. Dashed lines in figure 14 depict values of the electron temperature in the ionization layer predicted by the model [3, 44, 45]. There is good agreement between the two models at moderate T_w, especially at $U = 12$ V.

Thus, the present results qualitatively agree with those given by the simplified model [3, 44, 45], and in the case of an atmospheric-pressure argon plasma at moderate U the agreement is not only qualitative but also quantitative. It should be emphasized that this conclusion conforms to the discussion of physical justification of the two models given in the preceding sections: the case of an atmospheric-pressure argon plasma at moderate U is the only one where both models are reasonably well justified.

4. Comparison with the experiment

There are a variety of methods of experimental investigation of plasma–cathode interaction in high-pressure arc discharges, including spectroscopic measurements of plasma parameters in the near-cathode region, determination of the near-cathode voltage drop by means of electrostatic probe measurements and pyrometric measurements of the cathode surface temperature. A comparison between the theory and the experiment has been performed by different authors, e.g. [16] and references therein. In all cases the comparison was limited to integral characteristics, such as the near-cathode voltage drop or total heat losses.

A considerable amount of data on distributions of plasma parameters in the near-cathode region, in particular, of the electron temperature and/or density, has been obtained by spectroscopic measurements, e.g. [47–58] and references therein. Measured maximum electron temperatures in the near-cathode region varied over a wide range depending on experimental conditions and on the mode of operation of the cathode; for example, values of 9×10^3 K and 3.6×10^4 K have been reported in [56] and respectively, [58]. A comparison of the experiment with a theory has been virtually inexistent up to now: there is not much sense in comparing results of spatially resolved measurements with theoretical values obtained by means of separate treatments of different sub-layers with a spatially uniform electron temperature governed by an equation of integral balance. The present model gives distributions of parameters across the near-cathode layer and therefore represents a first step in the direction to make such a comparison meaningful. The second, and final, step will consist of combining the present model with the model of nonlinear surface heating (e.g. [16] and references therein), which will allow one to simulate the plasma–cathode interaction as a whole and thus to find the distribution of parameters not only across the near-cathode layer but along the cathode surface as well. Until this second step has been completed, distributions of the electric current density and temperature along the cathode surface remain unknown; hence any comparison will be inconclusive. Nevertheless some useful information can be extracted even at the present stage.

Unfortunately, there are no data on very high-pressure mercury discharge, for which the hydrodynamic theory should work best. Let us consider spectroscopic measurements [56], which were performed with high spatial resolution in argon at pressures from 1 to 3 bar and in which the electron temperature was deduced from Boltzmann plots of population densities and the electron density was determined from measured continuum intensities. No data on the temperature of the cathode surface nor on the near-cathode voltage are available in the paper [56]; however, such data have been reported in preceding papers from the same group. For example, the temperature of the cathode tip for the plasma pressure $p = 2.6$ bar, cathode height of 20 mm and radius of 0.5 mm and the arc current of 4 A can be taken from figure 8(a) of [59] and equals 3000 K. The near-cathode voltage drop for these conditions can be taken from figures 2(a) or 7 of [60] and equals 15 V.

Simulations for the above-mentioned conditions performed with $T_w = 3000$ K have shown that U equal to 15 V corresponds to $j_c = 4.14 \times 10^5$ A m^{-2}. Distributions of n_e and T_e obtained with these values of T_w and j_c are shown in figure 15 by solid lines. (The parameter r_c was set equal to 0.5 mm in these calculations.) Note that the ratio j_{em}/j_c for these conditions is 1.04, so these conditions, in spite of j_c being low in absolute terms, should be considered similar to conditions of figure 5(b) rather than to those of 5(a). Also shown in figure 15 are experimental data referring to the axis of the discharge taken from figure 11 of [56]. The range of distances from the cathode surface in this figure is limited by the cathode radius (0.5 mm); in fact, the approximation of locally 1D (or, more precisely, spherically symmetric) current transfer, which is used in the modelling, loses its validity at even smaller x. The discrepancy between the theoretical and experimental data on the electron temperature is about 20%.

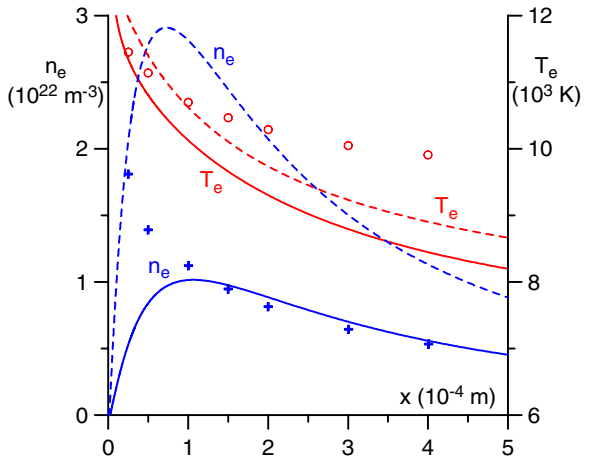

Figure 15. Lines: calculated distributions of the electron temperature and density in the near-cathode region. Argon. Lines: modelling, $p_0 = 2.6$ bar. Solid: $T_w = 3000$ K, $j_c = 4.14 \times 10^5$ A m^{-2}. Dashed: $T_w = 3140$ K, $j_c = 1.15 \times 10^6$ A m^{-2}. Points: experimental data from [56], $p = 2.6$ bar, $I = 4$ A. Circles: T_e. Crosses: n_e.

The discrepancy between data on the electron density is small at $x \gtrsim 100\ \mu$m, however reaching a factor of about 3 at smaller distances. As x decreases, the calculated function $n_e(x)$ attains a maximum value at $x \approx 100\ \mu$m, while the measured function monotonically increases in the whole range of x investigated (down to 25 μm).

A weak point of the above comparison is that the accuracy of experimental determination of T_w is insufficient to justify the use of the measured value of T_w as an input parameter. Another set of calculations has been performed in this connection. First, the diffuse mode of plasma–cathode interaction in the above-described conditions has been calculated for the arc current of 4 A by means of the Internet tool [34], which is a Fortran code based on the model of nonlinear surface heating combined with the model [3, 44, 45] for the near-cathode plasma layer. (The near-cathode voltage of 15.2 V was found, which is pretty close to the above-mentioned experimental value of 15 V.) The current density of 1.15×10^6 A m^{-2} and the surface temperature of 3190 K were found at the centre of the front surface of the cathode. Simulations performed by means of the present model with these values of j_c and T_w gave a value of $U = 8.9$ V, i.e. too low, but a little smaller $T_w = 3140$ K gave the right value $U = 15$ V. Distributions of n_e and T_e obtained with the latter values of T_w and j_c are shown in figure 15 by the dashed lines. The discrepancy between the theoretical and experimental data on the electron temperature is now about 10%. However, the theoretical data on n_e deviate from the experiment more strongly than the data depicted by the solid lines, although the discrepancy is still within a factor of about 3. The maximum of the function $n_e(x)$ has shifted to smaller x; however this shift is insufficient. In other words, the course of the distribution $n_e(x)$ remains problematic.

Obviously, the above comparison is inconclusive and will have to be revisited after the present model has been combined with the model of nonlinear surface heating. If the deviation between the theory and the experiment on the distribution of the electron density persists, it will be an indication of the necessity to re-analyse kinetic and/or transport coefficients of the electrons and/or the role of molecular ions, or maybe even of the fact that the diffusion approach is insufficient to very accurately describe the relaxation of a beam of electrons emitted by the cathode on distances that small.

While analysing spectroscopic results [56] by means of the model of nonlinear surface heating, one should keep in mind the following. In the framework of this model, the near-cathode voltage drop is assumed to be constant along the cathode surface, so the highest value of the current density occurs at the hottest point of the cathode surface. The latter is the edge of the front surface, where conditions for thermal-conduction heat removal are the worst and the surface temperature is about 20 K higher than that at the centre of the front surface, as the calculations by means of the code [34] show for the conditions of experiment [56]. (The figure of 20 K refers to a cathode with a flat front surface. If a rounding of the edge of the cathode is taken into account, the hottest point will still remain on the rounded part, although the temperature difference with respect to the centre of the front surface will decrease: 10 K for the radius of rounding of 100 μm.) A higher value of j_c at the edge will result in higher values of both T_e and n_e at distances of interest from the cathode surface (tens of micrometres and higher). However, the measurements [56] have shown the opposite trend: T_e and n_e in the diffuse mode have maxima at the centre of the front surface of the cathode rather than at the edge.

This contradiction may be explained as follows. First, increases in T_w and j_c affect distributions $T_e(x)$ and $n_e(x)$ in the opposite directions: while an increase in j_c enhances T_e and n_e, an increase in T_w causes a reduction in T_e and n_e. Therefore, an increase in T_e and n_e at the edge of the front surface which is caused by an increase in j_c is partially compensated by a decrease in T_e and n_e caused by an increase in T_w. Second, the present model allows one to obtain an order-of-magnitude estimate of the voltage drop in the constriction zone: it is given by the potential difference between the point separated from the cathode by a distance equal to, say, the cathode radius and the edge of the near-cathode layer identified as described in section 3.2. This potential difference is about 1 V in the above-described simulations for the conditions of the experiment [56]. One could think therefore that the voltage applied to the near-cathode layer at the centre of the front surface of the cathode will be a bit higher than that applied at the edge, and this effect will be sufficient to ensure higher T_e and n_e. Therefore, the model of nonlinear surface heating may have to be supplemented by a calculation of the potential variation in the constriction zone while being used for analysis of the experiment [56].

5. Conclusions

A 1D model of the near-cathode region in high-pressure arc discharges has been developed. The model is based on the hydrodynamic (diffusion) approach and treats the whole near-cathode region in a unified way, without assumptions of thermal or ionization equilibrium or quasi-neutrality.

Transport of the plasma species is described by the Stefan–Maxwell equations, a description which is valid at arbitrary ionization degree of the plasma in contrast to a description based on Fick's law for the ions and the electrons which is valid provided that the ionization degree is low enough. Boundary conditions taking into account emission of the electrons by the cathode surface are formulated. Transport, kinetic and radiation coefficients of the plasma are evaluated and a method of numerical solution of the obtained nonlinear boundary-value problem (which is quite stiff) developed. Numerical results are reported for very high-pressure mercury arcs, which are typical of high-intensity discharge lamps, and for an argon arc at atmospheric pressure, which is a kind of standard high-pressure arc, and include distributions of plasma parameters across the near-cathode region, CVCs, and energy flux from the plasma to the cathode.

Analysis of numerical results has allowed us to identify physical mechanisms dominating different parts of the near-cathode region and thus to pin down different sub-layers. The following sub-layers have been identified in the case of very high-pressure mercury arcs: the region of radiation-dominated LTE plasma, the layer of thermal perturbation, the layer of thermal non-equilibrium and the space-charge sheath. These sub-layers may also be identified in the case of an atmospheric-pressure argon arc at intermediate and high current densities (although the region of radiation-dominated LTE plasma is not very well pronounced at intermediate current densities); additionally, one can also introduce in this case an ionization layer, thus arriving at a structure similar to the one proposed previously for a near-anode region in high current arcs [35, 36].

Energy flux from an arc plasma to the surface of a thermionic cathode must be sufficient to heat the surface up to temperatures necessary for sufficiently strong thermionic emission. Values of the energy flux that high are ensured by a strong input of electrical energy into the electron gas occurring in the space-charge sheath. This input results in a maximum of the electron temperature in the sheath. The energy received by the electron gas is spent for ionization; thus ion current to the cathode is generated, which is needed to sustain current transfer. These results confirm the point of view according to which a space-charge sheath is of primary importance in near-cathode layers of high-pressure arc discharges. While previously this point of view was supported by arguments based on a treatment of sub-layers and involving ion bombardment as a dominating mechanism of heating of the cathode (e.g. [16] and references therein), in this work this point of view is supported by a straightforward numerical modelling of a collision-dominated near-cathode region.

It should be stressed that regimes in which the sheath plays a minor role are in principle possible; however, they do not occur under conditions of high-pressure arc discharges. In other words, local values of the temperature and the current density at each point of the arc attachment self-adjust in such a way that there is a space-charge sheath with a sufficiently strong power input, and the latter occurs, according to the present numerical results, when the local current density exceeds the electron emission current or is slightly below it.

The hydrodynamic (diffusion) description of motion of the ions and the electrons, employed in this work in the whole near-cathode region, including the space-charge sheath, is justified in the case of a very high-pressure mercury plasma. In the case of an atmospheric-pressure argon plasma, this description remains reasonably well justified at the intermediate current density, but not at the high current density.

The present analysis has confirmed the assumption of the primary importance of the space-charge sheath, which constitutes a physical basis of most of the simplified models of the near-cathode region in high-pressure arc discharges (e.g. [3, 44, 45], [9] and [11]), as well as a number of other assumptions employed by these models. In summary, these models are reasonably well justified in the case of an atmospheric-pressure argon plasma at moderate values of the near-cathode voltage drop, and some of these models remain justified at high values also; however, the simplified models are unjustified in the case of a very high-pressure mercury plasma. The latter is due to two factors: (1) the very large number of collisions suffered by an ion while crossing the space-charge sheath in a very high-pressure mercury plasma invalidates the assumption of collision-free motion of the ions in the sheath, employed by the above-mentioned simplified models; (2) the separate treatment of a quasi-neutral ionization layer and a space-charge sheath with frozen ionization and recombination, employed by the simplified models, is unjustified in the case of a very high-pressure mercury plasma since the ion current to the cathode in this case is generated at least partly inside the space-charge sheath.

A comparison of results given by the present model with those given by the simplified model [3, 44, 45] has revealed qualitative agreement. In the case of an atmospheric-pressure argon plasma at moderate values of the near-cathode voltage drop the agreement is not only qualitative but also quantitative.

The present model, being the first one to predict not only integral characteristics of the plasma–cathode interaction but also distributions of plasma parameters across the near-cathode layer, represents a first step to a meaningful theoretical analysis of results of spectroscopic measurements of plasma parameters in the near-cathode region. Unfortunately, there are no experimental data on a very high-pressure mercury discharge, for which the hydrodynamic theory should work best, and the comparison is limited to the measurements in argon [56]. There is good agreement, to about 10–20%, between the modelling and the experiment as far as the electron temperature is concerned. However, the calculated electron density distribution reveals a maximum at about 100 μm from the cathode surface which is not observed in the experiment; as a consequence, there is a discrepancy of about a factor of 3 between the data on the electron density. This question will have to be revisited after the uncertainty in distributions of the electric current density and temperature along the cathode surface has been removed by combining the present model with the model of nonlinear surface heating.

Acknowledgments

This work was supported by the projects POCI/FIS/60526/2004 and PPCDT/FIS/60526/2004 *Modes of Current Transfer to*

Cathodes of High-Pressure Arc Discharges and Their Stability of FCT, POCI 2010 and FEDER and by the project *Centro de Ciências Matemáticas* of FCT, POCTI-219 and FEDER.

Appendix A. Transport, kinetic and radiation coefficients

Let us start with the evaluation of the transport coefficients appearing in the set of equations formulated in section 2.1. The binary diffusion coefficients are expressed as

$$D_{\alpha\beta} = \frac{3\pi}{32}\left(\frac{8kT_{\alpha\beta}}{\pi m_{\alpha\beta}}\right)^{1/2}\frac{1}{n\bar{Q}^{(1,1)}_{\alpha\beta}}, \tag{45}$$

where $\bar{Q}^{(1,1)}_{\alpha\beta}$ are the energy-averaged cross sections for momentum transfer in collisions of particles of species α and β, which are related to the energy-dependent cross sections for momentum transfer, $Q^{(1)}_{\alpha\beta}(\varepsilon)$, by the formula

$$\bar{Q}^{(1,1)}_{\alpha\beta} = \frac{1}{2(kT_{\alpha\beta})^3}\int_0^\infty \varepsilon^2 \exp\left(-\frac{\varepsilon}{kT_{\alpha\beta}}\right) Q^{(1)}_{\alpha\beta}(\varepsilon)\,\mathrm{d}\varepsilon. \tag{46}$$

Note that the quantity $(8kT_{\alpha\beta}/\pi m_{\alpha\beta})^{1/2}$ represents the mean relative speed of particles of species α and β.

The average cross section $\bar{Q}^{(1,1)}_{\mathrm{ia}}$ of ion–atom collisions is a function of T_h and is evaluated by means of an analytical formula which is taken from [5] (for mercury) or obtained by fitting the data [61] extended to higher temperatures by means of results [5] (for argon). Note that the ion distribution function is assumed to be a Maxwellian function with a temperature equal to that of neutral atoms, which implies that the work of the electric field over the ion mean free path is considerably smaller than the thermal energy of the neutral atoms.

The electron–atom cross section $\bar{Q}^{(1,1)}_{\mathrm{ea}}$ is a function of T_e and is tabulated by numerically evaluating the integral (46). The energy-dependent cross section for momentum transfer in electron–atom collisions, $Q^{(1)}_{\mathrm{ea}}(\varepsilon)$, is taken from [62, 63] or [64] for collisions of electrons with atoms of argon or mercury, respectively.

Electron–ion collisions are governed by the Coulomb interaction. Averaging of the energy-dependent electron–ion cross section (e.g. [27]) by means of equation (46) gives

$$\bar{Q}^{(1,1)}_{\mathrm{ei}} = \frac{e^4 \ln\Lambda}{32\pi\varepsilon_0^2(kT_\mathrm{e})^2}. \tag{47}$$

Here $\ln\Lambda$ is the Coulomb logarithm ($\Lambda = 1.24\times 10^7 T_\mathrm{e}^{3/2} n_\mathrm{e}^{-1/2}$, where T_e is in K and n_e in m^{-3} [27]).

It is seen from the above that the binary diffusion coefficients may be introduced in numerical simulations in a simple and practical way, which is a consequence of the fact that $nD_{\alpha\beta}$ is a function of only one variable $T_{\alpha\beta}$. (nD_{ei} represents an exception: in addition to a dependence on T_e, it depends weakly on n_e via the Coulomb logarithm. However, it may be evaluated by means of simple analytical formulae (45) and (47).) General procedures of calculation of most of the other transport coefficients (e.g. [27]) are considerably more complex and their use for the purposes of this work is not warranted. In this work, such coefficients are either replaced by their limiting values corresponding to limiting cases of partially or strongly ionized plasmas or are interpolated between these values. Note that the limiting cases of partially or strongly ionized plasmas are defined here by inequalities $\bar{\nu}_{\mathrm{ea}} \gg \bar{\nu}_{\mathrm{ei}}$ or, respectively, $\bar{\nu}_{\mathrm{ea}} \ll \bar{\nu}_{\mathrm{ei}}$, where $\bar{\nu}_{\mathrm{ea}} = n_\mathrm{a} C_\mathrm{e} \bar{Q}^{(1,1)}_{\mathrm{ea}}$ and $\bar{\nu}_{\mathrm{ei}} = n_\mathrm{i} C_\mathrm{e} \bar{Q}^{(1,1)}_{\mathrm{ei}}$ are average frequencies of momentum transfer in electron–atom and, respectively, electron–ion collisions. The interpolation is linear over the parameter P defined as $P = \bar{\nu}_{\mathrm{ea}}/\bar{\nu}_{\mathrm{ei}} = n_\mathrm{a} D_{\mathrm{ei}}/n_\mathrm{i} D_{\mathrm{ea}}$. Transport of electrons in partially ionized plasmas is described by Lorentzian formulae (e.g. [27, 25]). In this work, these formulae are used under the assumption of Maxwellian electron energy distribution, which is rigorously justified if $\bar{\nu}_{\mathrm{ee}}$, the average frequency of momentum transfer in electron–electron collisions, considerably exceeds $\bar{\nu}_{\mathrm{ea}} m_\mathrm{e}/m_\mathrm{a}$ and the electron Maxwellization length is much smaller than a characteristic scale of variation of parameters of the electron gas. Transport of electrons in strongly ionized plasmas is described by Spitzer and Härm formulae (e.g. [27]).

Let us proceed to the evaluation of the correction coefficients $C_{\alpha\beta}$. The coefficient C_{ia} is governed by the ion–atom interaction. Since the frequency of collisions of singly charged ions with atoms of a parent gas depends on the collision energy rather weakly, this coefficient may be set equal to unity. For the correction coefficients C_{ea} and C_{ei} values are assumed that correspond to the limiting cases of a partially or, respectively, strongly ionized plasma. This choice is based on the following. Equation (5) for the electrons (with $\alpha = \mathrm{e}$) contains a term that involves C_{ea} and is proportional to $(\boldsymbol{v}_\mathrm{e} - \boldsymbol{v}_\mathrm{a})$ and a term that involves C_{ei} and is proportional to $(\boldsymbol{v}_\mathrm{e} - \boldsymbol{v}_\mathrm{i})$. Taking into account that quantities C_{ea}, C_{ei} and $|\boldsymbol{v}_\mathrm{e} - \boldsymbol{v}_\mathrm{a}|/|\boldsymbol{v}_\mathrm{e} - \boldsymbol{v}_\mathrm{i}|$ are of the order unity, one finds that the ratio of the two above-mentioned terms is of the order of P. The above-described choice ensures that the value assumed for the coefficient C_{ea} is accurate just in that particular case where the term involving this coefficient is dominating, which is the case $P \gg 1$, i.e. the case of partially ionized plasma. Similarly, the coefficient C_{ei} is accurate in the particular case of strongly ionized plasma, $P \ll 1$, where the term involving this coefficient is dominating. In other words, the above-described choice of coefficients C_{ea} and C_{ei} ensures correct values of the friction-force term of the transport equation for the electrons in both limiting cases of partially and strongly ionized plasmas.

In accord with the above, C_{ea} is obtained as the ratio of the diffusion coefficient D_{ea} evaluated in the first approximation of the Chapman–Enskog method to that evaluated by means of the Lorentzian formula with the Maxwellian electron energy distribution function:

$$C_{\mathrm{ea}} = \frac{9\pi(kT_\mathrm{e})^2}{32\bar{Q}^{(1,1)}_{\mathrm{ea}}\int_0^\infty \varepsilon\,[Q^{(1)}_{\mathrm{ea}}(\varepsilon)]^{-1}\exp(-\varepsilon/kT_\mathrm{e})\,\mathrm{d}\varepsilon}.$$

The correction coefficient C_{ei} in a strongly ionized plasma with singly charged ions may be found as the ratio of the diffusion coefficient D_{ea} evaluated in the first approximation of the Chapman–Enskog method to that obtained by means of the Spitzer and Härm formula and equals 0.506.

The thermal diffusion coefficients $C^{(\mathrm{h})}_\mathrm{i}$ and $C^{(\mathrm{h})}_\mathrm{a}$ are governed by ion–atom collisions. Once again taking into

account that the frequency of collisions of singly charged ions with atoms of a parent gas depends on the collision energy rather weakly, we set $C_i^{(h)} = C_a^{(h)} = 0$, i.e. assume that transport equations (5) for the heavy particles do not contain terms proportional to ∇T_h. The coefficients $C_\alpha^{(e)}$ are evaluated by means of the interpolation expression (e.g. [65])

$$C_e^{(e)} = \frac{1}{1+P}C_{tdei} + \frac{P}{1+P}C_{tdea}, \quad C_i^{(e)} = -\frac{n_e}{n_i}\frac{1}{1+P}C_{tdei},$$
$$C_a^{(e)} = -\frac{n_e}{n_a}\frac{P}{1+P}C_{tdea}, \tag{48}$$

where C_{tdei} and C_{tdea} are the values of thermal diffusion coefficient for electrons, $C_e^{(e)}$, in the limits of strongly and partially ionized plasmas, respectively. The coefficient C_{tdea} is evaluated by means of the expression

$$C_{tdea} = \frac{\int_0^\infty \varepsilon\,[Q_{ea}^{(1)}(\varepsilon)]^{-1}(\varepsilon/kT_e - 5/2)\,\exp(-\varepsilon/kT_e)\,d\varepsilon}{\int_0^\infty \varepsilon\,[Q_{ea}^{(1)}(\varepsilon)]^{-1}\exp(-\varepsilon/kT_e)\,d\varepsilon},$$

which follows from the Lorentzian formulae with the Maxwellian electron energy distribution. The coefficient C_{tdei} for plasmas with singly charged ions may be found by means of the Spitzer and Härm formulae and equals 0.703.

The thermal diffusion part of the density of heat flux transported by the electrons, $\boldsymbol{h}_e$, is evaluated in terms of the same coefficients that govern the thermal diffusion force for electrons

$$A_i^{(e)} = \frac{1}{1+P}C_{tdei}, \qquad A_a^{(e)} = \frac{P}{1+P}C_{tdea}. \tag{49}$$

The thermal conductivity of electrons is given by the interpolation expression

$$\kappa_e^{-1} = \kappa_{ea}^{-1} + \kappa_{ei}^{-1}. \tag{50}$$

The thermal conductivity κ_{ea} of electrons in the limiting case of partially ionized plasma is obtained by means of the Lorentzian formula with the Maxwellian electron energy distribution and may be written as

$$\kappa_{ea} = C_{therm}kn_e\frac{nD_{ea}}{C_{ea}n_a}, \tag{51}$$

where the coefficient C_{therm} is

$$C_{therm} = \frac{\int_0^\infty \varepsilon\,[Q_{ea}^{(1)}(\varepsilon)]^{-1}(\varepsilon/kT_e - 5/2)^2\exp(-\varepsilon/kT_e)\,d\varepsilon}{\int_0^\infty \varepsilon\,[Q_{ea}^{(1)}(\varepsilon)]^{-1}\exp(-\varepsilon/kT_e)\,d\varepsilon} - C_{tdea}^2. \tag{52}$$

The thermal conductivity κ_{ei} of the electrons in the limiting case of strongly ionized plasma with singly charged ions may be found by means of the Spitzer and Härm formulae:

$$\kappa_{ei} = 3.20\,kn_e nD_{ei}/n_i. \tag{53}$$

The coefficients $A_a^{(h)}$ and $A_i^{(h)}$ determining the thermal diffusion part of the heat flux transported by heavy particles, being proportional to, respectively, $C_a^{(h)}$ and $C_i^{(h)}$, are set equal to zero. In other words, the heat flux $\boldsymbol{h}_{hp}$ is assumed to be entirely due to heat conduction.

The thermal conductivity κ_{hp} of heavy particles is given by the sum of contributions due to atoms and ions

$$\kappa_{hp} = \kappa_a + \kappa_i, \tag{54}$$

each contribution being evaluated using interpolation expressions analogous to equation (50) (e.g. [66]):

$$\kappa_a = \frac{75k}{64\bar{Q}_{aa}^{(2,2)}}\left(\frac{\pi kT_h}{m_a}\right)^{1/2}\left(1 + \frac{n_i\bar{Q}_{ia}^{(2,2)}}{n_a\bar{Q}_{aa}^{(2,2)}}\right)^{-1}, \tag{55}$$

$$\kappa_i = \frac{75kn_i}{64\bar{Q}_{ia}^{(2,2)}n_a}\left(\frac{\pi kT_h}{m_a}\right)^{1/2}\left(1 + \frac{n_i\bar{Q}_{ii}^{(2,2)}}{n_a\bar{Q}_{ia}^{(2,2)}}\right)^{-1}. \tag{56}$$

The average cross sections $\bar{Q}_{aa}^{(2,2)}$ and $\bar{Q}_{ia}^{(2,2)}$ for argon are evaluated by means of formulae obtained by fitting the data [61]: $\bar{Q}_{aa}^{(2,2)} = 1.12\times10^{-18}T_h^{-0.2}$, $\bar{Q}_{ia}^{(2,2)} = 3.6\times10^{-18}T_h^{-0.3}$ (T_h is in K and $\bar{Q}_{ia}^{(2,2)}$ in m^2). The average cross section $\bar{Q}_{aa}^{(2,2)}$ for mercury is estimated on the basis of data on the thermal conductivity of LTE mercury plasma given in [67]. In the temperature range 3000–5000 K, where $\kappa_e, \kappa_i \ll \kappa_a$ and $n_i\bar{Q}_{ia}^{(2,2)} \ll n_a\bar{Q}_{aa}^{(2,2)}$, these data have been analysed by means of equation (55) without the third multiplier on the right-hand side and it was found that $\bar{Q}_{aa}^{(2,2)}$ for mercury exceeds the corresponding cross section for argon by a factor which is approximately constant and equal to 1.15, i.e. $\bar{Q}_{aa}^{(2,2)} = 1.29\times10^{-18}T_h^{-0.2}$ for mercury. The latter formula is also used in this work outside the above-mentioned temperature range. The ratio of the resonant charge exchange cross sections [5] for mercury and argon is virtually independent of the collision energy and approximately equals 2.9. It is therefore assumed that $\bar{Q}_{ia}^{(2,2)}$ for mercury exceeds the corresponding cross section for argon by a factor of 2.9, i.e. $\bar{Q}_{ia}^{(2,2)} = 1.04\times10^{-17}T_h^{-0.3}$ for mercury. The average cross section $\bar{Q}_{ii}^{(2,2)}$ is evaluated by means of the expression [66]

$$\bar{Q}_{ii}^{(2,2)} = \frac{e^4\ln\Lambda}{36\pi\varepsilon_0^2(kT_h)^2}. \tag{57}$$

The ionization rate constant k_i is represented as the sum of rate constants of direct and stepwise ionization: $k_i = k_{dir} + k_{step}\beta$. Expressions for k_{dir} and k_{step} are taken from [5]. The factor $\beta = n_e/(n_e + n_e^{(0)})$ approximately accounts for the decrease in the rate of stepwise ionization due to radiation escape. The latter comes into play at n_e of the order of $n_e^{(0)}$ or below, where $n_e^{(0)}$ is estimated using the balance equation for the first excited state: at $n_e = n_e^{(0)}$ the rate of de-excitation of this state by electron impact equals the rate of de-excitation due to radiation escape evaluated taking into account the radiation trapping in a plasma of radius of about 1 mm. $n_e^{(0)}$ estimated in such a way equals 10^{21} m^{-3} for argon and 10^{19} m^{-3} for mercury. The recombination rate coefficient is evaluated by means of the formula $k_r = (k_{dir} + k_{step})(n_e^2/n_a)_S$, where $(n_e^2/n_a)_S$ is the ratio n_e^2/n_a evaluated under the assumption of ionization equilibrium, i.e. by means of the Saha equation, and represents a function of T_e.

At sufficiently high n_e, the rate of radiation energy losses, w_{rad}, is close to its value in LTE plasma. The radiation

energy losses in LTE atmospheric-pressure plasma for a wide temperature range have been calculated taking into account both continuum and line radiation in [68–70] for Ar and in [67, 71] for Hg. These data are fitted by means of the following formulae, which take into account the fact that the net emission coefficient is approximately proportional to the plasma pressure p (e.g. [29, 67, 70]) and apply to argon and, respectively, mercury plasmas of a radius of about 1 mm:

$$w_{\mathrm{rad}} = 2.6 \times 10^{25} \frac{p}{T_{\mathrm{e}}^{2.52}} \exp\left(-\frac{1.69 \times 10^5}{T_{\mathrm{e}}}\right), \tag{58}$$

$$w_{\mathrm{rad}} = 6.3 \times 10^{22} \frac{p}{T_{\mathrm{e}}^{2.32}} \exp\left(-\frac{8.32 \times 10^4}{T_{\mathrm{e}}}\right). \tag{59}$$

Here p is in bar, T_{e} in K and w_{rad} in W m^{-3}.

Since the radiation losses come into play in an outer section of the near-cathode region where n_{e} is high, the above formulae are, in principle, sufficient for the purposes of this work. However, these formulae would give unrealistic results if applied to an inner section of the near-cathode region, where T_{e} can be very high while n_{e} low. At low n_{e} the radiation losses are due to radiation of excited atomic states. A simple estimate may be obtained by assuming that the de-excitation of the radiating atomic state due to radiation escape prevails over the de-excitation in collisions with electrons. Then the radiation losses are governed by the rate of excitation of these states by electron impact and may be approximately written as

$$w_{\mathrm{rad}} = k_1 n_{\mathrm{a}} n_{\mathrm{e}} \, \Delta E, \tag{60}$$

where ΔE is the excitation energy of the first excited atomic state and k_1 is the effective rate constant of excitation of this state which is evaluated as described in [5]. Note that this expression is accurate if $n_{\mathrm{e}} \ll n_{\mathrm{e}}^{(0)}$ and represents an upper estimate otherwise. An approximate procedure of evaluation of w_{rad} at an arbitrary n_{e} consists of a linear interpolation between equation (60) and equation (58) or (59) over the parameter $(n_{\mathrm{e}}/n_{\mathrm{e}}^{(0)})^2$.

Appendix B. Method of numerical solution

The governing differential equations are transformed to a system of four ordinary differential equations of second order. This is done as follows. Eliminating J_{a} from equation (5) for ions and electrons by means of equation (19) and J_{i} by means of expression $J_{\mathrm{i}} = J_{\mathrm{e}} + j/e$, one gets

$$[(n_{\mathrm{a}} + n_{\mathrm{i}})R_{\mathrm{ia}} + (n_{\mathrm{e}} - n_{\mathrm{i}})R_{\mathrm{ei}}]J_{\mathrm{e}} - [(n_{\mathrm{a}} + n_{\mathrm{i}})R_{\mathrm{ia}} + n_{\mathrm{e}}R_{\mathrm{ei}}]\left(-\frac{j}{e}\right)$$
$$= -(n_{\mathrm{i}}kT_{\mathrm{h}})' + n_{\mathrm{i}}eE - C_{\mathrm{i}}^{(\mathrm{h})} n_{\mathrm{i}} k T_{\mathrm{h}}' - C_{\mathrm{i}}^{(e)} n_{\mathrm{i}} k T_{\mathrm{e}}', \tag{61}$$

$$[(n_{\mathrm{a}} + n_{\mathrm{e}})R_{\mathrm{ea}} + (n_{\mathrm{i}} - n_{\mathrm{e}})R_{\mathrm{ei}}]J_{\mathrm{e}} - n_{\mathrm{e}}(R_{\mathrm{ea}} - R_{\mathrm{ei}})\left(-\frac{j}{e}\right)$$
$$= -kT_{\mathrm{e}}n_{\mathrm{e}}' - n_{\mathrm{e}}eE - \tilde{C}_{\mathrm{e}}^{(e)} n_{\mathrm{e}} k T_{\mathrm{e}}', \tag{62}$$

where a prime denotes differentiation with respect to x, $R_{\alpha\beta} = kT_{\alpha\beta}C_{\alpha\beta}/nD_{\alpha\beta}$, and $\tilde{C}_{\mathrm{e}}^{(e)} = C_{\mathrm{e}}^{(e)} + 1$. Solving equation (62) for J_{e}, substituting the result into equation (1) for electrons and eliminating n_{i} by means of equation (17), one gets

$$\left[B\frac{-kT_{\mathrm{e}}n_{\mathrm{e}}' - n_{\mathrm{e}}eE - \tilde{C}_{\mathrm{e}}^{(\mathrm{e})} n_{\mathrm{e}} k T_{\mathrm{e}}' + n_{\mathrm{e}}(R_{\mathrm{ea}} - R_{\mathrm{ei}})\left(-\frac{j}{e}\right)}{(n_{\mathrm{a}} + n_{\mathrm{e}})R_{\mathrm{ea}} + \frac{\varepsilon_0}{Be}(BE)'R_{\mathrm{ei}}}\right]'$$
$$= B\left(k_{\mathrm{i}}n_{\mathrm{a}}n_{\mathrm{e}} - k_r n_{\mathrm{e}}^3 - \frac{\varepsilon_0}{Be}k_r n_{\mathrm{e}}^2 (BE)'\right). \tag{63}$$

Equation (63) represents a second-order differential equation for n_{e}.

Combining equations (61) and (62) in order to eliminate J_{e} and then eliminating n_{i} by means of equation (17), one gets

$$\left[\frac{\varepsilon_0 k T_{\mathrm{h}}}{Be}(BE)' - \frac{\varepsilon_0}{B^2}\frac{(BE)^2}{2} + n_{\mathrm{e}}kT_{\mathrm{h}}\right]'$$
$$= \frac{2\varepsilon_0 E^2}{r_{\mathrm{c}}\sqrt{B}} - (C_{\mathrm{i}}^{(\mathrm{h})} k T_{\mathrm{h}}' + C_{\mathrm{i}}^{(e)} k T_{\mathrm{e}}')\frac{\varepsilon_0}{Be}(BE)'$$
$$+ \left[R_{\mathrm{ia}}\frac{\varepsilon_0}{Be}(BE)' - n_{\mathrm{e}}(X_1 R_{\mathrm{ea}} - R_{\mathrm{ia}} - X_2 R_{\mathrm{ei}})\right.$$
$$\left. + n_{\mathrm{a}}R_{\mathrm{ia}}\right]\left(-\frac{j}{e}\right) + X_1 k T_{\mathrm{e}} n_{\mathrm{e}}' + X_2 n_{\mathrm{e}} eE + X_1 \tilde{C}_{\mathrm{e}}^{(e)} n_{\mathrm{e}} k T_{\mathrm{e}}'$$
$$- (C_{\mathrm{i}}^{(\mathrm{h})} k T_{\mathrm{h}}' + C_{\mathrm{i}}^{(e)} k T_{\mathrm{e}}')n_{\mathrm{e}}, \tag{64}$$

where

$$X_1 = \frac{\left[\left(n_{\mathrm{a}} + n_{\mathrm{e}} + \frac{\varepsilon_0}{Be}(BE)'\right)R_{\mathrm{ia}} - \frac{\varepsilon_0}{Be}(BE)'R_{\mathrm{ei}}\right]}{\left[(n_{\mathrm{a}} + n_{\mathrm{e}})R_{\mathrm{ea}} + \frac{\varepsilon_0}{Be}(BE)'R_{\mathrm{ei}}\right]},$$
$$X_2 = X_1 + 1. \tag{65}$$

Equation (64) represents a second-order differential equation for E. Note that the terms of this equation that involve E are small in the major part of the near-cathode plasma (outside the space-charge sheath); the only exception is the term $X_2 n_{\mathrm{e}} eE$, and it is this term that makes equation (64) appropriate for numerical determination of the electric field in a plasma with a high degree of quasi-neutrality [72], in contrast to the original Poisson equation (17).

Second-order differential equations for T_{e} and T_{h} are obtained substituting equations (15) and (16) into equations (10) and (11).

An iterative algorithm is used to solve the formulated system of equations. The equations are linearized with the use of Newton's method and at each step of the iteration process are solved jointly by means of the Petukhov method [73] (which is a method of numerical solution of a boundary-value problem for a linear ordinary differential equation of the second or third order or for a partial differential equation of the parabolic type, based on a finite-difference scheme of the fourth order of accuracy) generalized for the

case of a system of equations. All regions of fast variation of the solution must be resolved to ensure convergence of the iterations, which requires a numerical grid with a variable step.

References

[1] Zhou X and Heberlein J 1994 *Plasma Sources Sci. Technol.* **3** 564–74
[2] Benilov M S 1995 *J. Phys. D: Appl. Phys.* **28** 286–94
[3] Benilov M S and Marotta A 1995 *J. Phys. D: Appl. Phys.* **28** 1869–82
[4] Rethfeld B, Wendelstorf J, Klein T and Simon G 1996 *J. Phys. D: Appl. Phys.* **29** 121–8
[5] Benilov M S and Naidis G V 1998 *Phys. Rev.* E **57** 2230–41
[6] Almeida R M S, Benilov M S and Naidis G V 2000 *J. Phys. D: Appl. Phys.* **33** 960–7
[7] Schmitz H and Riemann K U 2001 *J. Phys. D: Appl. Phys.* **34** 1193–202
[8] Benilov M S and Coulombe S 2001 *Phys. Plasmas* **8** 4227–33
[9] Schmitz H and Riemann K U 2002 *J. Phys. D: Appl. Phys.* **35** 1727–35
[10] Almeida N A, Benilov M S, Franklin R N and Naidis G V 2004 *J. Phys. D: Appl. Phys.* **37** 3107–16
[11] Lichtenberg S, Dabringhausen L, Langenscheidt O and Mentel J 2005 *J. Phys. D: Appl. Phys.* **38** 3112–27
[12] Benilov M S and Naidis G V 2005 *J. Phys. D: Appl. Phys.* **38** 3599–608
[13] Scharf F H and Brinkmann R P 2006 *J. Phys. D: Appl. Phys.* **39** 2738–46
[14] Benilov M S, Naidis G V, Petrovic Z L, Radmilovic-Radjenovic M and Stojkovic A 2006 *J. Phys. D: Appl. Phys.* **39** 2959–63
[15] Scharf F H, Oberrath J, Merthmann P and Brinkmann R P 2007 *Proc. 11th Int. Symp. on Science and Technol. of Light Sources (LS:11) (Shanghai, China, May 2007)* ed M Q Liu and R Devonshire (Sheffield, UK: FAST-LS) ISBN 978-0-9555445-0-7, pp 261–2
[16] Benilov M S 2008 *J. Phys. D: Appl. Phys.* **41** 144001
[17] Amakawa T, Jenista J, Heberlein J V R and Pfender E 1998 *J. Phys. D: Appl. Phys.* **31** 2826–34
[18] Haidar J 1999 *J. Phys. D: Appl. Phys.* **32** 263–72
[19] Benilov M S, Bochkarev G G and Rogov B V 1995 *IEEE Trans. Plasma Sci.* **23** 742–9
[20] Benilov M S, Bochkarev G G and Lyashko A V 1992 *High Temp.* **30** 527–32
[21] Kim H C, Iza F, Yang S S, Radmilovic-Radjenovic M and Lee J K 2005 *J. Phys. D: Appl. Phys.* **38** R283–301
[22] Hirschfelder J O, Curtiss C F and Bird R B 1964 *Molecular Theory of Gases and Liquids* (New York: Wiley)
[23] Monchick L, Munn R J and Mason E A 1966 *J. Chem. Phys.* **45** 3051–8
Monchick L, Munn R J and Mason E A 1968 *J. Chem. Phys.* **48** 3344 (erratum)
[24] Ferziger J H and Kaper H G 1972 *Mathematical Theory of Transport Processes in Gases* (Amsterdam: North-Holland)
[25] Zhdanov V M 2002 *Transport Phenomena in Multicomponent Plasma* (London: Taylor and Francis)
[26] Zhdanov V M and Tirskii G A 2003 *J. Appl. Math. Mech.* **67** 365–88
[27] Mitchner M and Kruger C H 1973 *Partially Ionized Gases* (New York: Wiley)
[28] Lowke J J 1970 *J. Appl. Phys.* **41** 2588–600
[29] Gleizes A, Gonzalez J J and Freton P 2005 *J. Phys. D: Appl. Phys.* **38** R153–183
[30] Arslanbekov R R and Kolobov V I 2003 *J. Phys. D: Appl. Phys.* **36** 2986–94
[31] Su C H and Lam S H 1963 *Phys. Fluids* **6** 1479–91
[32] Chung P M, Talbot L and Touryan K J 1975 *Electric Probes in Stationary and Flowing Plasmas: Theory and Application* (New York: Springer)
[33] Benilov M S 1988 *High Temp.* **26** 780–93
[34] http://www.arc_cathode.uma.pt
[35] Nemchinskii V A and Perets L N 1977 *Sov. Phys.—Tech. Phys.* **22** 1083–7
[36] Nemchinsky V A 2005 *J. Phys. D: Appl. Phys.* **38** 4082–9
[37] Benilov M S and Cunha M D 2003 *J. Phys. D: Appl. Phys.* **36** 603–14
[38] Bauer A and Schultz P 1954 *Z. Phys.* **130** 197–211
[39] Li H P and Benilov M S 2007 *J. Phys. D: Appl. Phys.* **40** 2010–17
[40] Benilov M S 2000 *J. Phys. D: Appl. Phys.* **33** 1683–96
[41] Liu W F and Conway D C 1975 *J. Chem. Phys.* **62** 3070–3
[42] Biondi M A 1953 *Phys. Rev.* **90** 730–7
[43] Massey H 1976 *Negative Ions* (Cambridge: Cambridge University Press)
[44] Benilov M S and Cunha M D 2002 *J. Phys. D: Appl. Phys.* **35** 1736–50
[45] Benilov M S and Cunha M D 2003 *Phys. Rev.* E **68** 056407
[46] Benilov M S 1992 *IEEE Trans. Plasma Sci.* **20** 1047–52
[47] Haidar J and Farmer A J D 1993 *J. Phys. D: Appl. Phys.* **26** 1224–9
[48] Pellerin S, Musio K, Pokrzywka B and Chapelle J 1994 *J. Phys. D: Appl. Phys* **27** 522–8
[49] Haidar J and Farmer A J D 1994 *J. Phys. D: Appl. Phys.* **27** 555–60
[50] Haidar J 1995 *J. Phys. D: Appl. Phys.* **28** 2494–504
[51] Zhou X and Heberlein J 1996 *Plasma Chem. Plasma Process.* **16** 229s–244s
[52] Pokrzywka B, Musiol K, Pellerin S, Pawelec E and Chapelle J 1996 *J. Phys. D: Appl. Phys.* **29** 2644–9
[53] Bentley R E 1997 *J. Phys. D: Appl. Phys.* **30** 2880–6
[54] Dzierzega K, Pokrzywka B and Pellerin S 2004 *J. Phys. D: Appl. Phys.* **37** 1742–9
[55] Kühn G and Kock M 2006 *J. Phys. D: Appl. Phys.* **39** 2401–14
[56] Redwitz M, Langenscheidt O and Mentel J 2005 *J. Phys. D: Appl. Phys.* **38** 3143–54
[57] Kuhn G and Kock M 2007 *Phys. Rev.* E **75** 016406
[58] Mitrofanov N K and Shkol'nik S M 2007 *Tech. Phys.* **52** 711–20
[59] Dabringhausen L, Nandelstädt D, Luhmann J and Mentel J 2002 *J. Phys. D: Appl. Phys.* **35** 1621–30
[60] Nandelstädt D, Redwitz M, Dabringhausen L, Luhmann J, Lichtenberg S and Mentel J 2002 *J. Phys. D: Appl. Phys.* **35** 1639–47
[61] Devoto R S 1973 *Phys. Fluids* **16** 616–23
[62] Itikawa Y (ed) 2000 *Photon and Electron Interactions with Atoms, Molecules and Ions. Subvolume A Interactions of Photons and Electrons with Atoms* (*Numerical Data and Functional Relationships in Science and Technology* vol 17A) (Berlin: Springer)
[63] Phelps A V Ftp://jila.colorado.edu/collision_data/eletrans.txt Last revision May 21, 2005
[64] McEachran R P and Elford M T 2003 *J. Phys. B: At. Mol. Opt. Phys.* **36** 427–41
[65] Rozhansky V A and Tsendin L D 1988 *Collisional Transport in a Partially Ionized Plasma* (Moscow: Energoatomizdat) (in Russian)
[66] Liu W S, Whitten B T and Glass I I 1978 *J. Fluid Mech.* **87** 609–40
[67] Zollweg R J 1978 *J. Appl. Phys.* **49** 1077–91
[68] Kovitya P and Lowke J J 1985 *J. Phys. D: Appl. Phys.* **18** 53–70
[69] Benoy D A, van der Mullen J A M and Schram D C 1993 *J. Phys. D: Appl. Phys.* **26** 1408–13

[70] Gleizes A, Gonzalez J J, Liani B and Raynal G 1993 *J. Phys. D: Appl. Phys.* **26** 1921–7

[71] Paul K C, Takemura T, Matsuno H, Hiramoto T, Dawson F, Gonzalez J J, Gleizes A, Zissis G, Erraki A and Lavers J D 2004 *IEEE Trans. Plasma Sci.* **32** 118–26

[72] Benilov M S and Tirskii G A 1979 *J. Appl. Math. Mech.* **43** 309–26

[73] Petukhov I V 1964 *Numerical Calculation of Two-Dimensional Flows in a Boundary Layer* (Moscow: Nauka) pp 304–25